PARTICLE DYNAMICS IN THE PLASMA SHEET

A

THESIS

Presented to the Faculty of the

University of Alaska in Partial Fulfillment

of the Requirements

for the Degree of

MASTER OF SCIENCE

by
John S. Wagner, B.S.

Fairbanks, Alaska

August 1978

PARTICLE DYNAMICS IN THE PLASMA SHEET

RECOMMENDED:

R Parthasarathy

Thomas D. Stark

Hilbert F. Belon

Joseph R Kan

Chairman, Advisory Committee

Joseph R. Kan

Head, Space Physics and Atmospheric Sciences Program

Director, Geophysical Institute

APPROVED:

Dean, College of Environmental Sciences

May 1, 1978

Date

Vice Chancellor for Research and Advanced Study

May 1, 1978

Date

ABSTRACT

Trajectories of charged particles in the tail region of the earth's magnetosphere are studied using a model magnetic field. The particles form a thin sheet-like structure in the magnetotail called the plasma sheet. It is shown that most trajectories are categorized by two dimensionless parameters. One of them is equal to the ratio of the cross-tail electric force to the magnetic force in the mid-plane and determines the maximum particle energization. The other parameter is the ratio of the plasma sheet thickness to the particle gyroradius in the midplane and determines the degree to which the particle motion is adiabatic. All previous attempts at studying trajectories in the magnetotail are shown to be applicable only over limited ranges of the two parameters. Hence those studies are combined into a common framework, and those trajectories which have not been studied previously are added for completeness.

ACKNOWLEDGMENTS

This thesis was written under the helpful guidance of my Advisory Committee consisting of Dr. S.-I. Akasofu, Prof. A. Belon, Dr. J. Kan, Prof. R. Parthasarathy, and Dr. T. Roberts. I especially thank Dr. S.-I. Akasofu and Dr. J. Kan for going out of their way to provide suggestions, discussions and helpful assistance. I would like to thank Mr. Joe Enzweiler for many useful ideas, discussions and manuscript editing. I owe special thanks to Ms. H. Horiuchi for drawing the figures and Ms. N. Walters for typing, and for cheerfully putting up with my endless revisions. The work reported here was supported in part by a grant from the National Aeronautics and Space Administration NSG-7281, State of Alaska funds, and in part by a grant from the National Science Foundation, Atmosphere Sciences Section, ATM 74-23832.

TABLE OF CONTENTS

LIST OF FIGURES

LIST OF TABLES

INTRODUCTION

The tenuous plasma populating the magnetotail and the plasma sheet is largely collisionless. Hence an understanding of the motions of individual charged particles in those regions is an important first step in understanding the collective dynamics of the magnetotail plasma as a whole. But even this first step is difficult due to the staggering complexity and variety of the particle orbits found in the tail. The equations of motion are far too complex to be solved analytically, although a number of authors have attempted analytical solutions through the application of various approximations. Among them Speiser (1965a), Alexeev and Kropotkin (1970), and Sonnerup (1971) have approximated solutions in the high energy, or highly non-adiabatic limit. At the other extreme Stern and Palmadesso (1975), and Stern (1977) have attempted solutions in the low energy or adiabatic limit. Other authors have attempted to numerically integrate the equations of motion, for example Speiser (1965b), Cowley (1971), Eastwood (1972), Pudovkin and Tsyganenko (1973), and Swift (1977). Unfortunately, due to the assumptions made in those studies, each author dealt only with a limited variety of trajectories, and, therefore, their conclusions cannot be generalized to all conditions that may occur in the magnetotail.

In this thesis, a comprehensive numerical analysis of all possible magnetotail particle orbits is presented. The previous works are incorporated into a new classification scheme, and the apparent disagreements of the previous authors are resolved. The new classification makes use of the dimensionless equations of motion suggested by Swift (1977). The overall morphology of the orbits is shown to be determined by the dimensionless parameters found in the new equations of motion. An approximate invariant is found, which is the particle gyroradius computed in an ExB reference frame. The invariant is used to predict particle energization for all untrapped particles in the tail. The invariant is also used to spell out the limitations of Speiser's (1971) concept of gyroconductivity. In addition, an important class of trapped orbits is presented which suggests the natural formation of a thin current layer within the plasma sheet, as a natural consequence of the trapped folded figure-eight orbits described.

THE MODEL AND THE BASIC EQUATIONS

To analyze the motion of a charged particle in the plasma sheet, we choose a field model in which the magnetic field and the electric field are given by

$$\vec{B} = B_{xo} \tanh (z/_L)\hat{x} + B_{zo}\,\hat{z} , \qquad (1)$$

$$\vec{E} = E_{yo}\,\hat{Y} \quad , \tag{2}$$

where the x axis is assumed to lie along the earth-sun line (positive towards the sun), and the y axis lies in the midplane of the plasma sheet and is parallel to the cross-tail current. The z axis is normal to the midplane to complete the right-handed cartesian coordinate system. Note that the magnetic field of the model depends only on the z coordinate and the electric field is uniform. The normal component of the magnetic field, B_{zo}, is taken to be constant. The length L can be regarded as the half-thickness of the plasma sheet since B_x approaches B_{xo} as z/L approaches unity.

The magnetic field in (1) is not a self-consistent solution of the Vlasov-Maxwell equations, but the field configuration described by (1) does resemble the two-dimensional analytic solution for the plasma sheet by Kan (1973) and the numerical solution by Toichi (1972). For the purpose of this study, the field model in (1) is adequate for examining trajectories of "test" particles.

The equation of motion for a charged particle in a magnetic and electric field is given by

$$m d\vec{v}/dt = q\,(\vec{v}\times\vec{B} + \vec{E}) \quad , \tag{3}$$

where $\vec{v}$ is the particle velocity, m and q are respectively the mass and charge of the particle. To numerically analyze the

behavior of a particle in the model field it is advantageous to rewrite (3) in dimensionless form. For this purpose we choose to scale the distance by the gyroradius ρ_o and the time by the inverse angular gyrofrequency τ_o based on the normal field component B_{zo} and the initial speed v_o of a particle, i.e.

$$\rho_o = \frac{mv_o}{qB_{zo}} \tag{4}$$

$$\tau_o = \frac{m}{qB_{zo}} \quad . \tag{5}$$

Now, the equation of motion in (3) can be written in component form as follows

$$\frac{dv_x^*}{dt^*} = v_y^* \tag{6}$$

$$\frac{dv_y^*}{dt^*} = B_x^* v_z^* - v_x^* + E^* \tag{7}$$

$$\frac{dv_z^*}{dt^*} = -B_x^* v_y^* \quad , \tag{8}$$

where $x^* = x/\rho_o$, $y^* = y/\rho_o$, $z^* = z/\rho_o$, $t^* = t/\tau_o$, $v^* = v/v_o$ and

$$B_x^* = (B_{xo}/B_{zo}) \tanh (z^*/L^*) \tag{9}$$

$$L^* = L/\rho_o \tag{10}$$

$$E^* = E_y/v_o B_{zo} \quad . \tag{11}$$

It will be shown that the main characteristics of a particle orbit are determined by the parameters E* and L*. The ratio B_{xo}/B_{zo}, although it does not play an important role in orbit morphology, determines the limiting angle of the magnetic field as z*/L* becomes greater than unity. For definiteness $B_{xo}/B_{zo} = 0.1$ is chosen to approximate the plasma sheet conditions.

Since the initial speed v_o of a particle has been chosen as the scale speed, the initial velocity of a particle is therefore a unit vector whose direction is to be specified as an initial condition. The initial energy of a particle is equal to unity in units of the initial particle kinetic energy. The simultaneous equations (6)-(8) are solved numerically by using Bulisch-Stoer (1966) rational function extrapolation.

ORBIT ANALYSIS

Particle orbits in the model plasma sheet will be analyzed through the parameters L* and E* defined in (10) and (11). It is convenient to divide L* values into three ranges, $L^* \ll 1$, $L^* \simeq 1$, and $L^* \gg 1$ for the distant-tail region, the mid-tail region and the near-earth tail region, respectively. The ranges of E*, which are of practical interest in studying the dynamics of the plasma sheet, are $E^* \ll 1$ and $E^* \gtrsim 1$ for the quiet and disturbed conditions of the tail, respectively. Thus, there are six possible pairs of L* and E* in the ranges mentioned above. They will be designated as Cases 1 through 6 as follows: Case 1, $L^* \ll 1$ and $E^* \ll 1$; Case 2, $L^* \simeq 1$ and $E^* \ll 1$; Case 3, $L^* \gg 1$ and $E^* \ll 1$; Case 4, $L^* \ll 1$ and $E^* \gtrsim 1$; Case 5, $L^* \simeq 1$ and $E^* \gtrsim 1$; and Case 6, $L^* \gg 1$ and $E^* \gtrsim 1$.

The remaining portion of this section is devoted to discussing the properties of orbits in each of the six Cases. A comprehensive summary of the characteristics of particle orbits in the plasma sheet is then presented in Table I which also lists the previous studies to show how they fit into the overall picture of particle behavior in the plasma sheet.

Case 1 Orbits (L*<<1 and E*<<1)

Case 1 orbits are highly non-adiabatic. A typical orbit in this case is shown in Figure 1. The particle starts its orbit with initial energy 1 and pitch angle 180 degrees (antiparallel to $\vec{B}$). The particle is started well outside the plasma sheet at z* = 0.15; the values of L* and E* used were 0.1 and 0.05 respectively. Figure 1a is the top view of the orbit, projected into the x*-y* plane. The particle begins its orbit in the upper left corner of Figure 1a, at x* = 0, y* = 0. Figure 1b is a side view, showing the orbit as it follows a field line in the x*-z* plane. Figure 1c is an end view, looking earthward from the tail, in the y*-z* plane. In this example, and those that follow, the computed trajectories follow smooth curves. The plots are generated by straight line connections of consecutive particle positions in equal time intervals as indicated by the tic marks. Notice the net cross-tail displacement of $2\rho_o$ (just "2" in dimensionless coordinates). A strong similarity exists between such an orbit and the orbits discussed by Speiser (1965).

Table 1. TRAJECTORY SUMMARY

Key to Table:	L* / E*	Distant Tail $L^* \ll 1$	Mid-Tail $L^* \simeq 1$	Near Earth $L^* \gg 1$
1. Case 2. Trajectory Type 3. Maximum Cross-Tail Displacement 4. Maximum Lifetime in Plasma Sheet 5. Maximum Energy Gain 6. Previously studied by	Quiet Condition $E^* \ll 1$	1. I 2. Nonadiabatic, or Speiser type 3. $2\rho_o$ 4. $\pi\tau_o$ 5. $2q\rho_o E_y$ 6. Speiser (1965), Alexeev (1970), Sonnerup (1971)	1. II 2. Transitional type 3. $2\rho_o$ 4. Several Bounce Periods 5. $2q\rho_o E_y$ 6. Pudovkin et al. (1973), Swift (1977)	1. III 2. Adiabatic, or if trapped, "Folded Figure Eight" 3. $2\rho_o$ 4. $2L/v_o$ 5. $2q\rho_o E_y$ 6. Stern (1977)
	Disturbed Condition $E^* > 1$	1. IV 2. Energized, Non-adiabatic 3. $2\rho_o'$ (see note) 4. $\pi\tau_o$ 5. $2q\rho_o' E_y$ 6. Speiser (1967), Cowley (1971), Eastwood (1972)	1. V 2. Energized, Transitional 3. $2\rho_o'$ 4. Several Bounce Periods 5. $2q\rho_o' E_y$ 6. None	1. VI 2. Energized, Adiabatic 3. $2\rho_o'$ 4. $2L/v_o$ 5. $2q\rho_o' E_y$ 6. None

Note: $\rho_o' = (m/qB_{zo})(v_o + E_y/B_{zo})$

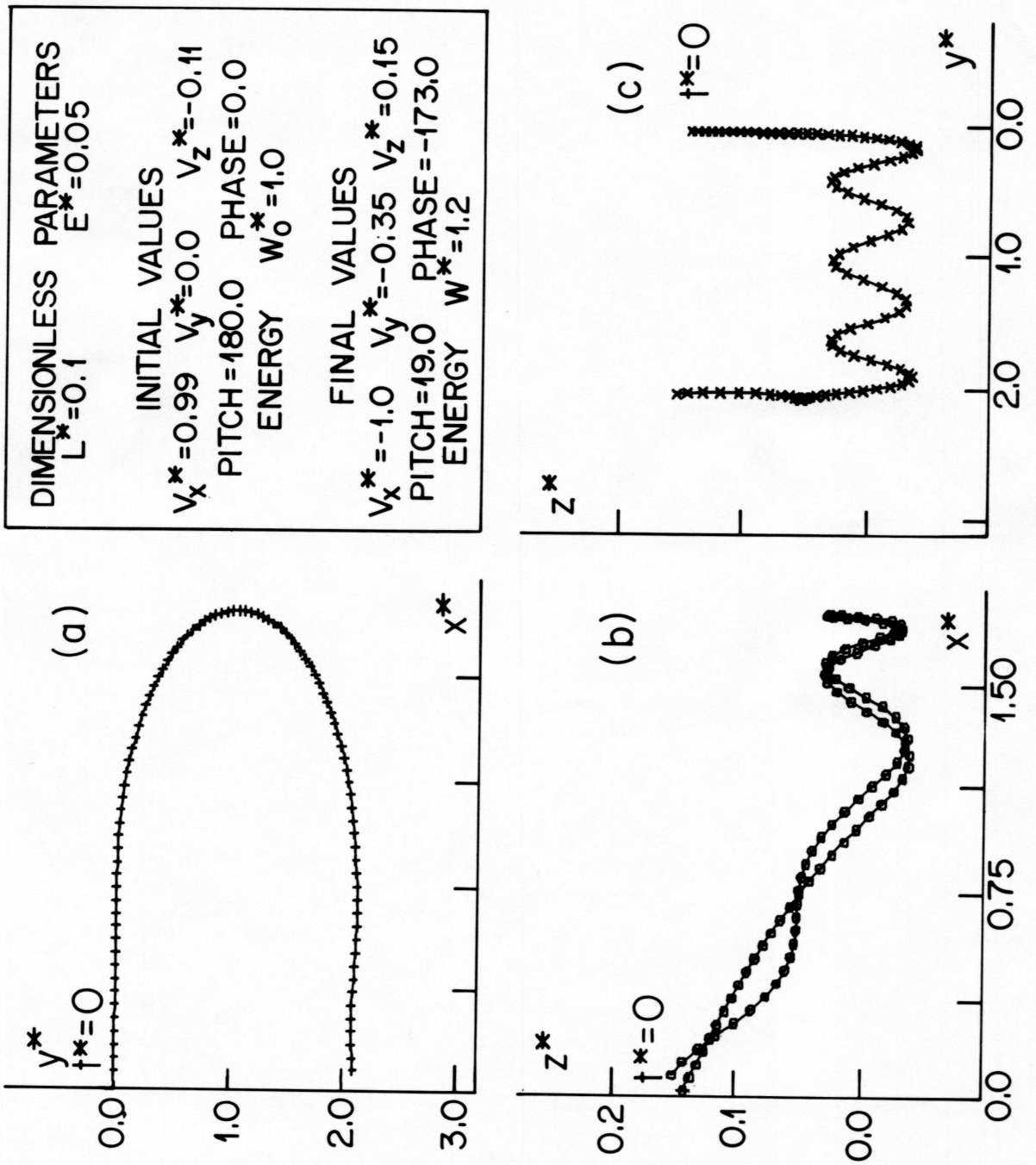

Figure 1 Projections of a Case 1 particle trajectory (untrapped) in a model plasma-sheet field

The energy gain is $4E^*(1 + E^*)$ and the total time spent in the plasma sheet is very close to $\pi\tau_o$ (or just "π"). In general, the cross-tail displacement, energy gain and containment time for all Case 1 orbits are found to be $2\rho_o$, $2q\rho_o E_y$ and $\pi\tau_o$, respectively, regardless of initial conditions (as long as the particle is started outside the sheet). Furthermore, it will be shown in the next sections that the above statements are true for Case 2 and 3 trajectories as well. In fact, the statement holds for Cases 4, 5 and 6 as long as the above quantities are measured in the proper (ExB) reference frame (this will be discussed in section 5).

Case 1 orbits can be either trapped or untrapped, but the trapped orbits are of little interest since they are confined to almost circular orbits in the mid-plane of the magnetotail. In fact, the trapping conditions for these orbits have been described by Sonnerup (1971). Case 1 trajectories can be expected to be found only in the distant magnetotail, when the cross-tail electric field is small. Particles with 5 kev energy in the distant tail (>60 R_E) where $B_z = 0.5\gamma$ and L = 1 R_E would have L* = 0.3. For an electric field of 1.5×10^4 volts/m., E* = 0.01. Higher energy particles would follow Case 1 orbits at distances closer to the earth.

Case 2 Orbits ($L^* \gtrsim 1$ and $E^* << 1$)

In general the motion of Case 2 trajectories includes a combination of features found in both the Case 1 (nonadiabatic) and Case 3 (adiabatic) which will be described in the next section. For this reason Case 2 orbits may be called transitional in nature.

Let us examine a typical Case 2 orbit with $L^* = 2.0$ and $E^* = 0.1$ as shown in Figure 2. The particle starts outside the plasma sheet at $z^* = 2.5$, with energy 1, and pitch angle 130 degrees. The particle gyrates adiabatically until it crosses the plasma sheet boundary ($z^* = L^*$). The particle continues adiabatic motion until it nears the mid-plane. The guiding center then disappears as the particle begins oscillating about the mid-plane, similar to the previously described Case 1 orbits. In general, the thickness of the region where the orbit can be said to resemble Case 1 orbits decreases with increasing L^*, as expected. While all Case 1 untrapped particles are quickly ejected from the plasma sheet as soon as the plane of the orbit has rotated 180 degrees around B_z, transitional Case 2 particles often leave the immediate vicinity of the mid-plane only temporarily, such as the example shown in Figure 2.

In many cases transitional particles are ejected in the same way as the Case 1 particle orbits, leaving the nonadiabatic region surrounding the mid-plane if the pitch angle is in the loss cone (see discussion of Case 3 orbits). If the pitch angle at the

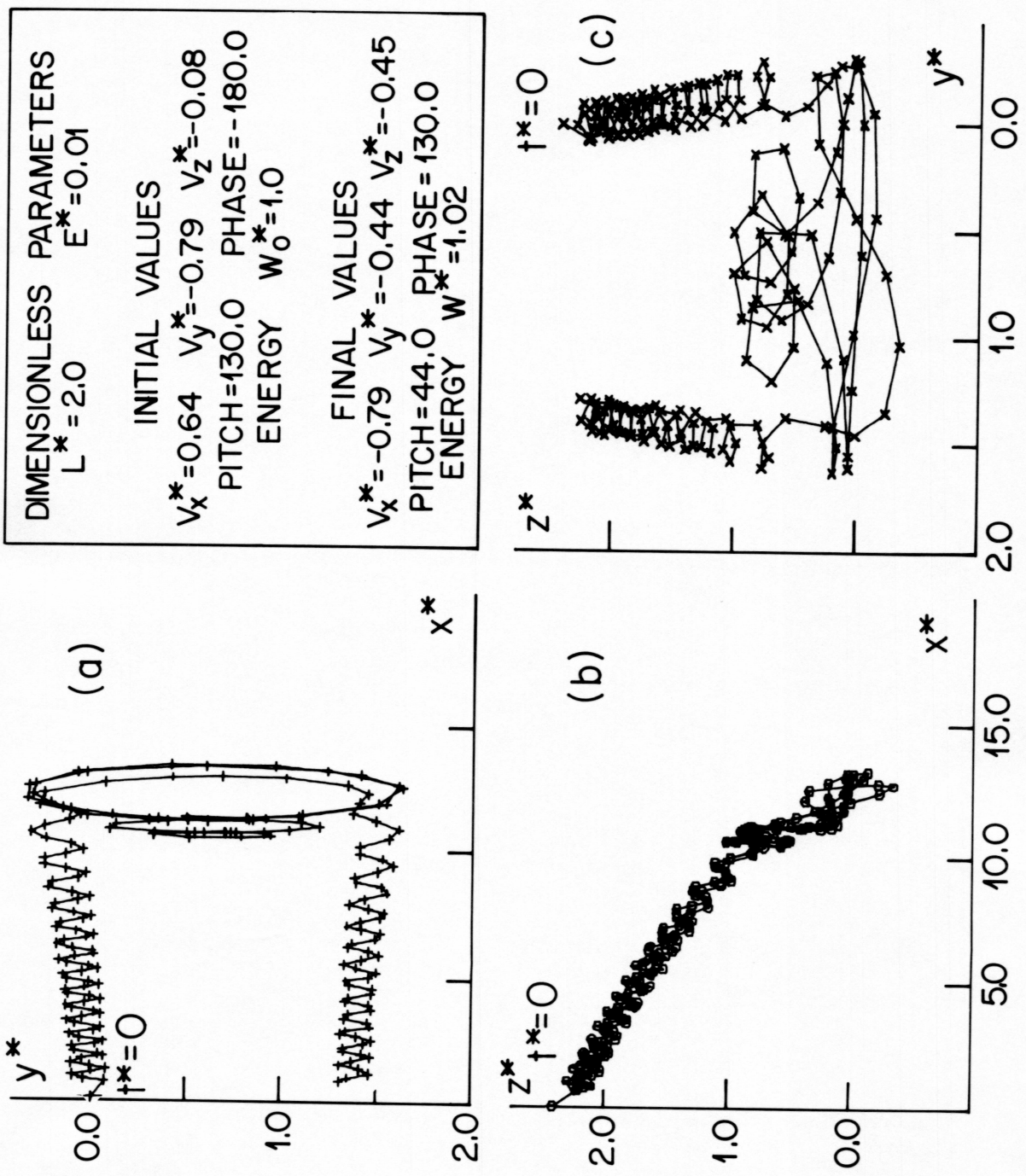

Figure 2 Projections of a Case 2 particle trajectory (untrapped) in a model plasma-sheet field

location where the particle leaves the nonadiabatic region is too large (and not in the loss cone) the particle cannot escape, but mirrors near the outer edge ($z^* \tilde{} L^*$) of the plasma sheet. The subsequent process of mirroring and reentering the mid-plane region continues until the particle's pitch angle is randomly scattered into the loss cone. Results show that even a fractional change in the initial phase angle will drastically change the orbit by altering the number of mirrorings. Hence the total time spent by the particles in the plasma sheet varies from a minimum of $\pi\tau_o$ (as in Case 1) to a maximum of several mean bounce periods within the plasma sheet. Surprisingly, however, the particle remains confined to a region having a cross-tail width of one gyrodiameter regardless of the complexity of the orbit. As can be seen in Figure 2, the maximum displacement is always one gyrodiameter. Similarly the maximum net energy gain is always $2q\rho_o E_y$.

Case 2 orbits may be expected to occur in the mid-tail region of the tail, a geocentric distance of (20-60 R_E). For example, a 5 kev particle in a field with $B_{zo} = 2\gamma$, and a plasma sheet thickness of I R_E would have $L^* = 1.8$, which falls into the Case 2 range. If there exists a cross-tail electric field of 1.5×10^{-4} volts/m. then E^* has a value of 0.1.

Case 3 Orbits ($L^*>>1$ and $E^*<<1$)

Orbits of this Case can be either trapped, as in Figure 3, or untrapped as in Figure 4. Unlike the trapped orbits of Cases 1 and 2, the trapped orbits in Case 3 are not confined to a thin region centered about the mid-plane of the plasma sheet. The Case 3 trapped orbits appear as folded figure eights. Note that the mid-plane crossing point does not shift across the tail. We shall point out later that Case 3 orbits are fundamental in understanding the structure of the near-earth plasma sheet, and explain the formation of the thin current sheet centered on the mid-plane.

Since Case 3 trajectories are nearly adiabatic, the conservation of μ (the magnetic moment) gives an expression specifying which orbits are trapped and which are untrapped. This expression is based on the particle's equatorial pitch angle α_o, as the particle crosses the mid-plane $z^* = 0$. The relationship is

$$\sin(\alpha_{loss}) = \frac{(B_{zo})^{\frac{1}{2}}}{(B_{zo}^2 + B_{xo}^2)^{\frac{1}{2}}} \qquad (12)$$

Those particles with an equatorial pitch angle less than that of the loss cone ($\alpha_o < \alpha_{loss}$) follow untrapped orbits as in Figure 4. Those trajectories with $\alpha_o > \alpha_{loss}$) are trapped as in Figure 3. The trapped orbits do not shift since B_{zo} is assumed constant in this paper. For the observed variations of B_{zo} in the tail the net cross-tail shift remains insignificant, as noted by Stern (1977).

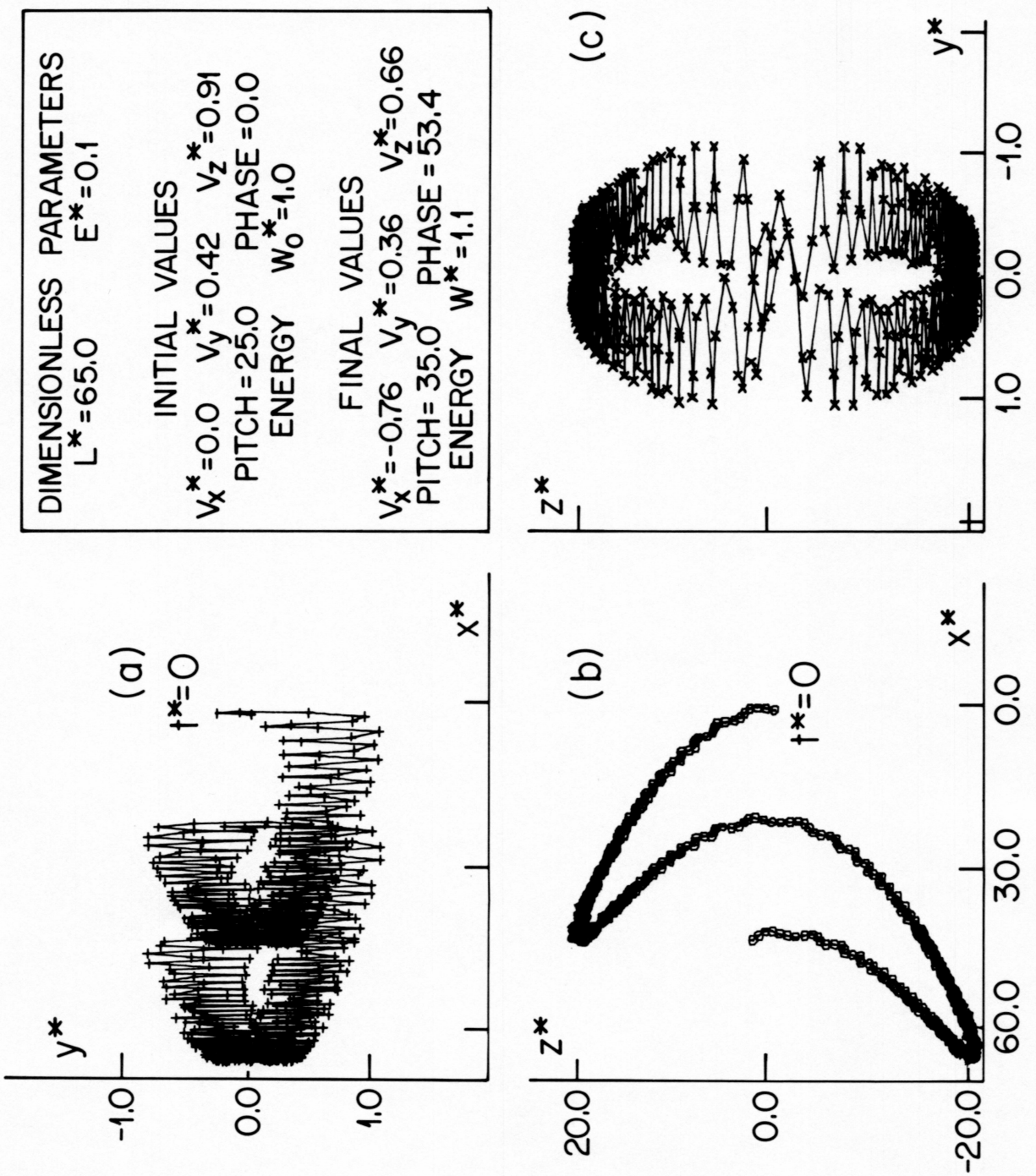

Figure 3 Projections of a Case 3 particle trajectory (trapped) in a model plasma-sheet field

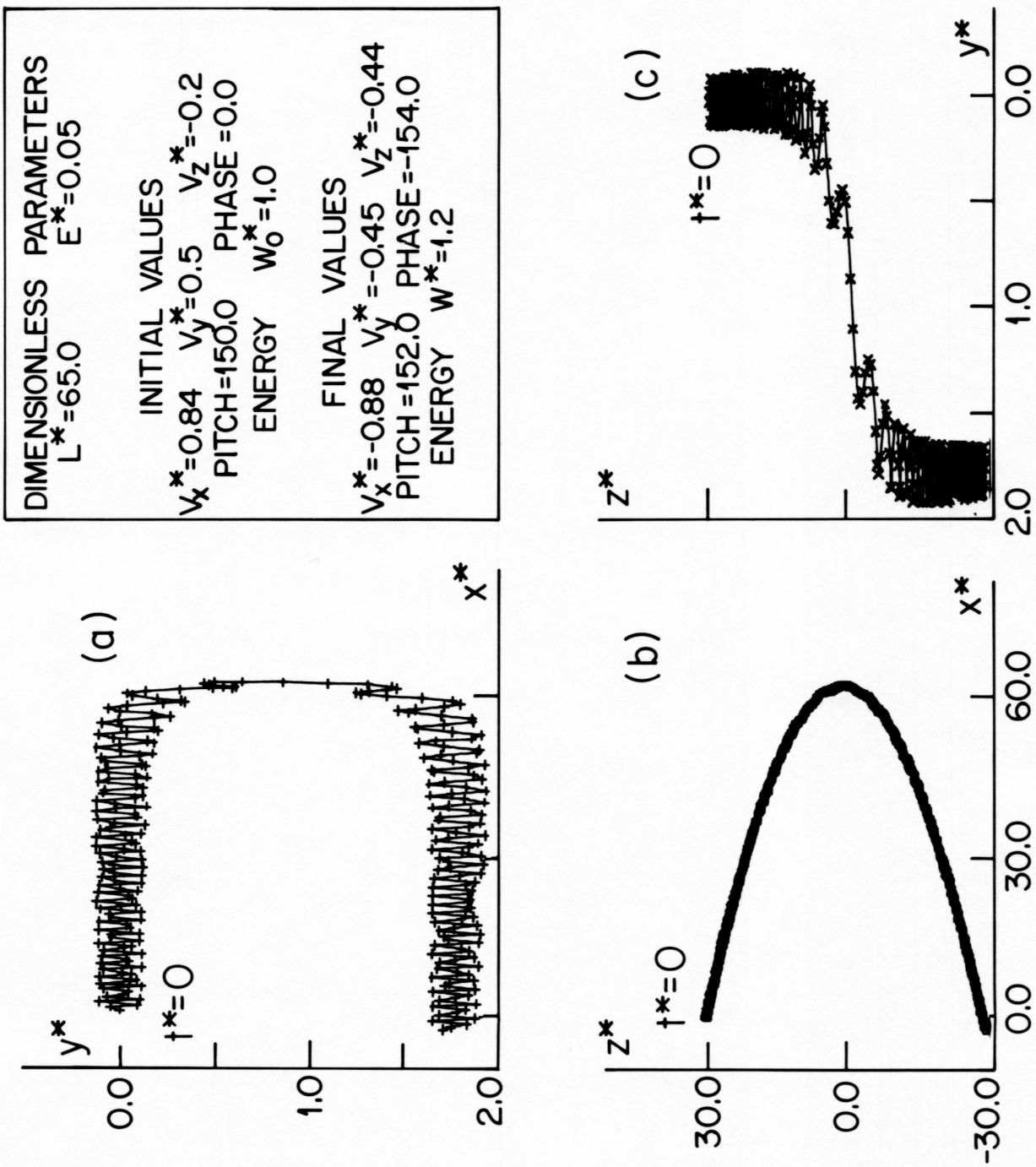

Figure 4 Projections of a Case 3 particle trajectory (untrapped) in a model plasma-sheet field

Let us examine first the representative Case 3 trapped orbit in Figure 3. The particle is started in the equatorial mid-plane $z^* = 0$ with energy 1 and pitch angle 25 degrees. The field parameters used are $L^* = 65$ and $E^* = 0.1$. The particle's guiding center spends most of its time in the mirroring process as illustrated, since the tic marks are spaced in equal time (every τ_o in Figure 3). In a thin layer surrounding the mid-plane the guiding center always crosses the mid-plane in the same direction and in a short period of time, around 1/100 of the total bounce time. The thickness of this particular region is roughly 1/10 of the total plasma sheet thickness. It is clear that the gradient drift is responsible for the displacement of $-2\rho_o$ during the mirroring process, and the curvature drift is responsible for the displacement of $+2\rho_o$ as the particle crosses the thin layer surrounding the mid-plane. The two drifts average out so that there is no cross-tail drift. Although the figure-eight orbits produce no net current across the tail, they do produce a thin current layer centered on the mid-plane. Particles near the outer edge of the plasma sheet are mirroring and their guiding center is moving slowly against the electric field. Particles near the mid-plane move rapidly along the electric field.

Finally, consider the typical untrapped orbit as in Figure 4. To illustrate the motion the particle is started inside the plasma sheet at $z^* = 30$. The field parameters chosen are $L^* = 65$ and $E^* = 0.05$. Notice the net displacement is once again $2\rho_o$ and the

energy gain is about $2q\rho_o E_y$. In general, for untrapped Case 3 orbits, the time spent in the plasma sheet is roughly $2L/v_{o''}$, which is simply the time it takes to travel a distance 2L with velocity the parallel component $v_{o''}$. In most cases $v_{o''}$ can be approximated by v_o.

All Case 3 orbits can be expected in the near-earth plasma sheet. For example, a particle with energy 2 kev in a field with $B_{zo} = 10\gamma$ and a sheet thickness of 10 R_E would have L* equal to 100. If the cross-tail electric field is 1.5×10^{-4} mv/m, the E* would be 0.05. Hence particles with these values of L* and E* follow Case 3 orbits.

Case 4 Orbits ($L^* \ll 1$ and $E^* \gtrsim 1$)

Case 4 trajectories are nonadiabatic, and considerably affected by the cross-tail electric field as shown in Figure 5. This is because the electric force on the particle is approximately equal to, or in the extreme case even greater than the magnetic force. Untrapped orbits in Case 4 resemble those of Case 1, except that the cross-tail electric field enhances the maximum displacement. The cross-tail displacement is $2\rho_o$ for Case 1 and $2\rho'_o$ for Case 4 orbits where ρ_o' is measured in a moving frame having an x-velocity of E_y/B_{zo}. This is discussed in detail in section 5. The result is that Case 4 particles are considerably energized by the electric field through an increased displacement along E_y. The maximum

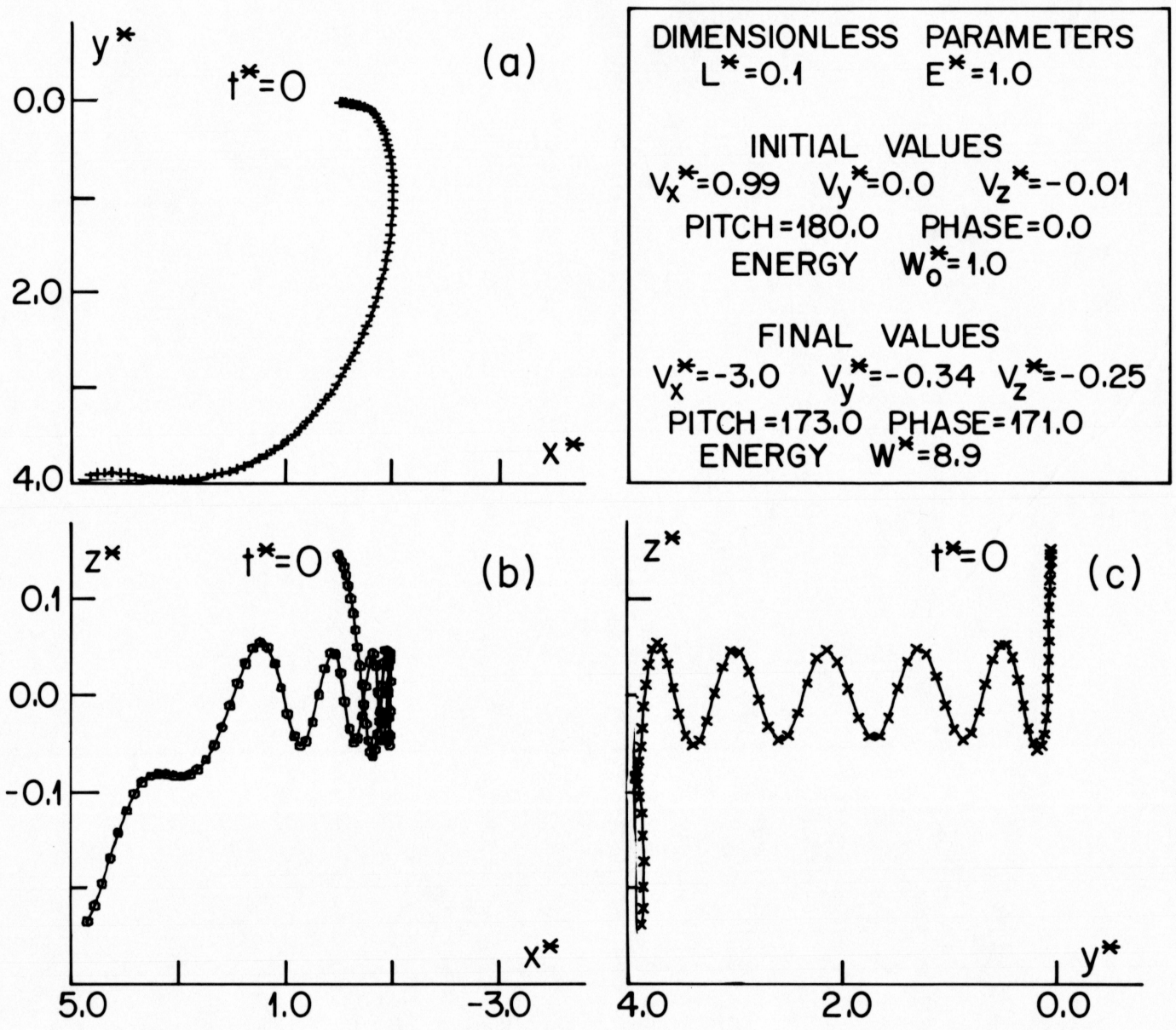

Figure 5 Projections of a Case 4 particle trajectory (untrapped) in a model plasma-sheet field

energization is $2q\rho_o' E_y$. The time spent in the plasma sheet remains $\pi\tau_o$ since the increased displacement is balanced by an increased velocity during energization to leave the total time unchanged.

The typical Case 4 orbit is shown in Figure 5. The conditions are the same as those in Figure 1, except that $E^* = 1$. From the figure it can be seen that the net displacement is enhanced to $4\rho_o$, or $2\rho_o'$ in the moving frame.

Case 4 orbits can be expected in the distant tail whenever a strong electric field is present.

Case 5 Orbits ($L^* \tilde{<} 1$ and $E^* \gtrsim 1$)

Case 5 orbits are the same as Case 2 but with an enhanced cross-tail displacement. One important effect of the large E^* is the reduction of time spent in the sheet. The time spent by a typical Case 5 particle in the plasma sheet is decreased when $E^* \gtrsim 1$ since ejection of the particle takes place after the first traversal through the plasma sheet. This is shown in Figure 6. Notice the particle is ejected with a net displacement of $4\rho_o$ or $2\rho_o'$ exactly as expected. The energization is also the same as in Case 4 and in Case 6.

These orbits should be found in the distant magnetotail whenever a large electric field is present.

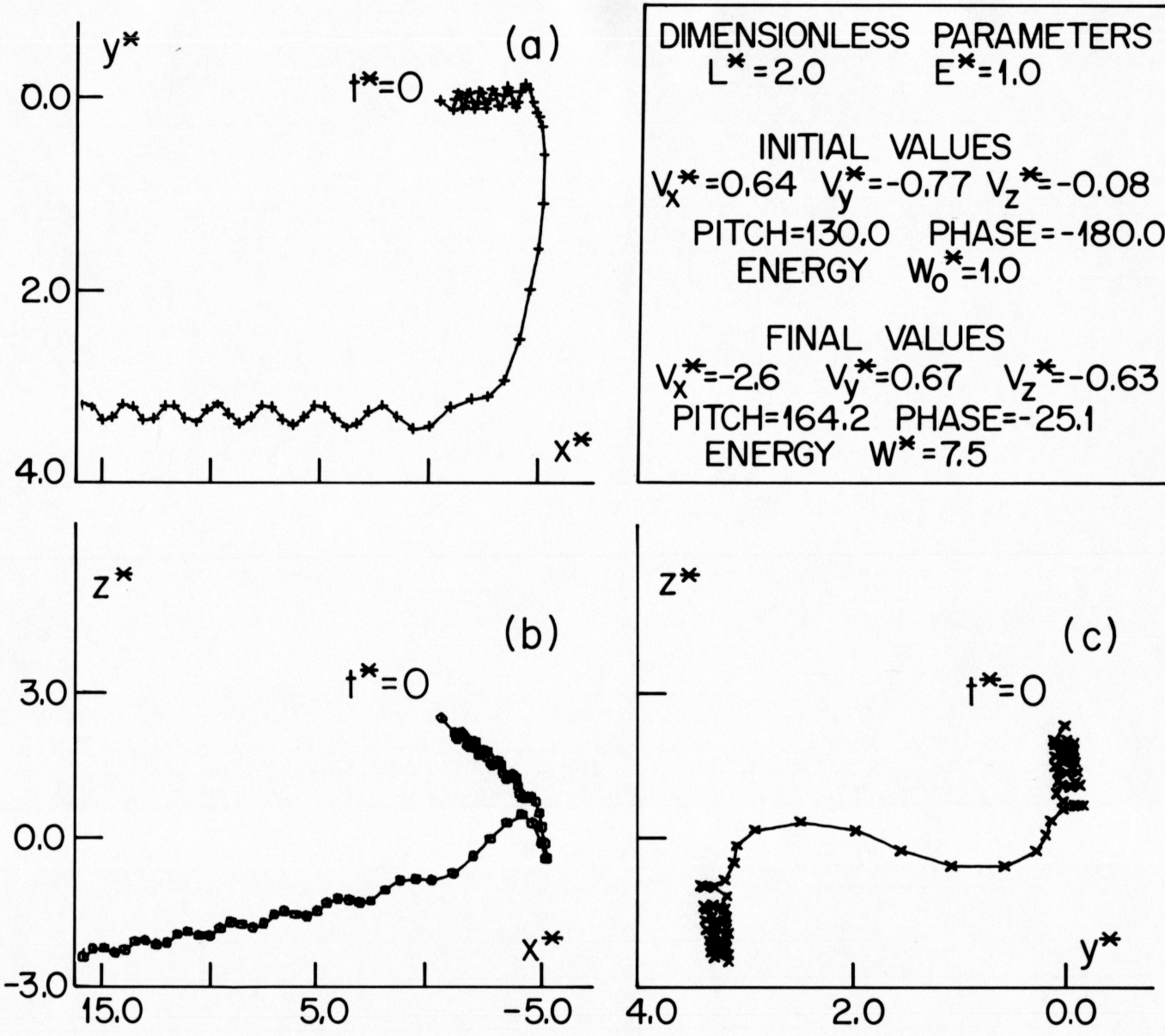

Figure 6 Projections of a Case 5 particle trajectory (untrapped) in a model plasma-sheet field

Case 6 Orbits ($L^* \ll 1$ and $E^* \gtrsim 1$)

Case 6 orbits are nearly adiabatic, but strongly affected by the cross-tail electric field. An example is shown in Figure 7, where the untrapped orbit is started at $z^* = 30$. The values of L^* and E^* are 65 and 1.0 respectively. Untrapped orbits in Case 6 show a maximum enhanced displacement of, once again, $2\rho_o'$, with the expected energization. Trapped orbits in Case 6 show a large E x B drift.

These orbits should be found in the near-earth magnetotail whenever a large cross-tail electric field is present. Lower energy particles would exhibit Case 6 motion farther out in the tail.

SUMMARY OF PREVIOUS WORK IN THE FRAMEWORK OF THE PRESENT STUDY

Analytical Approximations

Speiser (1965) was the first to attempt an analytical solution of the trajectory problem in the magnetotail. He examined magnetic field models both with and without a small B_z, and a small cross-tail E_y. Speiser tried to find an approximate solution to the differential equations of motion, and for simplicity he considered particles that were initially field aligned, entered the plasma sheet undergoing Case 1 motion, and were ejected. His solution does not yield trapped or drifting orbits, and is thus appropriately categorized with Case 1 untrapped orbits.

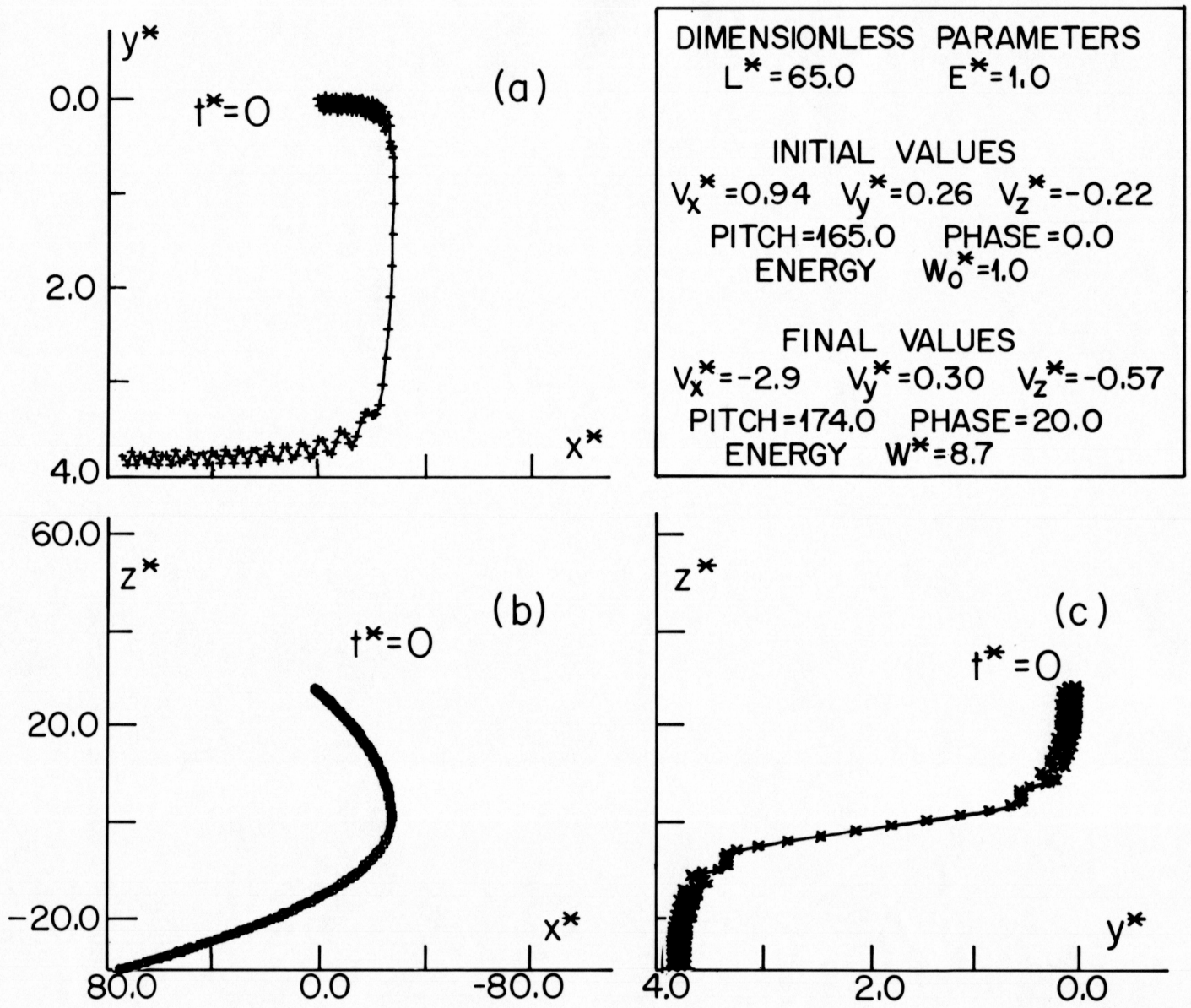

Figure 7 Projections of a Case 6 particle trajectory (untrapped) in a model plasma-sheet field

Alexeev and Kropotkin (1970) considered trajectories in an infinitely thin plasma sheet, with $L^* = 0$. They did not consider the effect of an electric field, and furthermore assumed $B_z << B_x$. Using geometrical arguments based on the continuity of the trajectory and particle velocity as the particle crosses the sharp plasma sheet boundary, they computed the number of mid-plane crossings, the total time spent in the mid-plane region, and the net cross-tail displacement. They arrived at the important conclusion that the maximum cross-tail displacement of particles entering the plasma sheet is $2\rho'_o$, or one gyrodiameter. This result, of course, appears to hold for a much broader range of orbits as we have demonstrated here.

Sonnerup (1971) considered several variations of plane symmetric tail-like fields. By using momentum and energy as constants of motion, he gave exact expressions for the turning points, oscillation period, drift velocity, and adiabatic invariant for a model with $B_{zo} = 0$. He considered all possible orbits in such a model, and defined "meandering orbits" as those which cross the mid-plane. All others are termed "drifting orbits." In the model in which Sonnerup included a normal magnetic field B_{zo}, he considered only guiding center motion, and made use of the second adiabatic invariant J. He solved for the approximate location of the turning points as they are projected into the x-y plane, and considered closed (trapped) orbits near the mid-plane, without considering either

the z-dependence of the orbit or the guiding center velocity and the period of the motion. In conclusion, Sonnerup's model with B_{zo} gives the x-y projected turning points of trapped particles in a field with L*<<1. These orbits are contained in Case 1, discussed earlier.

An entirely different type of trajectory occurs when a particle has L*>>1, and this is the type of guiding center motion discussed by Stern and Palmadesso (1975). They pointed out that the symmetric field of the magnetotail should be drift free for adiabatic particles and that the guiding center curvature and gradient drifts cancel when averaged over a trapped orbit. Stern (1977) also showed a net cross-tail drift should occur if B_z varies with x. In addition, he computed the average bounce period of drift free trapped orbits; however, he did not consider the effect of an electric field on particle behavior, untrapped adiabatic orbits, or nonadiabatic orbits. Thus, his orbits belong to Class 3.

Numerical Approximations

Speiser (1967) was also the first to numerically integrate the equations of motion of particles in the magnetotail. In terms of the parameters E* and L* his trajectories fall into Case 4 (untrapped). This is because Speiser used $B_{zo} = 10^{-2}\gamma$, making L* very small ($\sim$0.01); in addition, he used low energy (200 ev) particles, and an electric field of 3×10^{-4} volts/km, making his E* large, around one.

A numerical approach was also carried out by Cowley (1971), but his model did not include B_z. Therefore, his trajectories are applicable only in the presence of a neutral sheet, and always move transversely across the plasma sheet without being ejected.

Probably the most extensive numerical treatment of the orbit problem to date is that of Eastwood (1972, 1975). The majority of the trajectories Eastwood studied were of the Speiser type, Case 4. Eastwood used a B_z around 0.4γ, initial velocity 750 km/sec. and an electric field of 0.3 volts/ km. This gives $L^* = 10^{-4}$ and $E^* = 1$. He did notice that B_z plays a fundamental role in determining orbit morphology, and listed the types of orbits according to whether they were adiabatic, trapped, or coupled.

In their numerical approach, Pudovkin et al (1973) used values of $1 - 5\gamma$ for B_z. They used initial energies of 10 kev and electric fields around 0.3 volts/km. This gives $L^* \tilde{>} 1$ and $E^* \tilde{>} 1$, or Case 5.

Finally, Swift (1977), using a magnetic field model almost identical to the one in this paper, considered trajectories with $B_z = 5\gamma$, $E_y = 1.5$ volts/km and energies 75-400 ev. These correspond to Case 2 orbits. Swift's main emphasis is that magnetosheath particles become energized to plasma sheet energy as soon as they move across the plasma sheet and are ejected.

PARTICLE ENERGIZATION

In this section an argument is presented which uses a non-relativistic transformation to observe the magnetotail particle orbits in a moving frame. The speed of the frame is chosen so that no electric field is present in it. This argument is then used to show that the effects of an electric field can be predicted without numerical computation, as long as the orbits are known in the simple case when no electric field is present. Numerical computations support the argument.

The quantity E_y/B_{zo}, which is contained in the definition of E*, is the transformation velocity at which speed an earthward moving observer in the magnetotail would see no electric field. It turns out that as long as the transformation velocity is non-relativistic, the magnetic fields are identical in both the moving and earth-fixed systems. Any observer at rest in the earth frame and any observer in the moving frame must agree on the trajectory of any particle, as long as they take into account their relative motion. In fact, they must agree on the trajectory even though the moving observer believes the orbit to be determined solely by the magnetic field measured in the moving frame, and the earth-fixed observer believes the orbit to be due to the combination of electric and magnetic fields in the earth frame. The lack of an electric field in the moving frame is compensated for by the fact that the velocity of the particle in the moving frame is different

from the velocity measured in the earth frame, by an amount E_y/B_{zo} (measured in the x-direction).

Therefore, trajectory calculations really only need to be made in the simple case when no electric field is present. By assuming the trajectory has been computed in the moving reference frame, the effect of any electric field can be recovered.

For instance, it has been shown in the previous section that all untrapped orbits in the plasma sheet are displaced one gyrodiameter across the tail when there is no electric field present (see the discussion of Cases 1, 2 and 3). It has also been shown that the displacement is enhanced if the electric field is large enough so that $E^* \gtrsim 1$ (see Cases 4, 5 and 6). On the basis of the above consideration, the enhanced displacement can now be predicted without laborious numerical work.

Suppose the initial velocity along a field line for an untrapped particle in the earth frame is v_o (away from the earth). Then the initial velocity in the moving frame is $v_o' = v_o + E_y/B_{zo}$. Now in the moving frame where the particle has the higher velocity v_o', there is no electric field. For this reason the cross-tail displacement in the moving frame will simply be one gyrodiameter ($2\rho_o'$) based on the initial velocity v_o', where

$$\rho_o' = \frac{mv_o'}{qB_{zo}} \tag{13}$$

$$= \frac{m}{qB_{zo}} \left(v_o + \frac{E_y}{B_{zo}}\right) . \tag{14}$$

Of course, the cross-tail displacement must be the same in both coordinate systems since the displacement is perpendicular to the relative motion for the two systems. Hence the cross-tail displacement in the earth frame can be predicted even when there is an electric field present, and it is simply one gyrodiameter ($2\rho_o'$) measured in the $E_y \times B_{zo}$ reference frame.

Thus, the maximum energization ΔW, of a particle as it displaces $2\rho_o'$ along the cross-tail electric field E_y, can now be computed in terms of E*. The quantity $2q\rho_o'E_y$ is just expanded using the fact that W_o, the initial kinetic energy, is just $\frac{1}{2}mv_o^2$. The energization is then

$$\Delta W = 2q\rho_o'E_y \tag{15}$$

$$= 2qE_y \left(\frac{m}{qB_{zo}} \left(v_o + \frac{E_y}{B_{zo}}\right)\right) \tag{16}$$

$$= 4W_o E^* (1 + E^*) \quad , \tag{17}$$

recalling $E^* = E_y/v_o B_{zo}$.

DISCUSSION OF THE CROSS-TAIL CURRENT

Aside from a basic understanding of trajectory morphology, and a physical intuition of particle behavior in the magnetotail, this trajectory study was undertaken in an attempt to answer two important questions. The first question concerns the relationship

between the cross-tail current and the cross-tail electric field. For example, does the electric field drive any current, and if it does, how does it compare to the total current producing the curl of $\vec{B}$? The second question deals with the primary current carrier. Specifically, is the cross-tail current primarily carried by electrons or ions?

In recent years, a false sense of confidence has developed by proponents of the single particle approach because of its considerable success in modeling the ring current and the radiation belts. In most cases the success of the modeling has rested on two facts, namely that the particles in the plasma under study were behaving adiabatically, and in addition, they were producing only minor perturbations to the surrounding electric and magnetic fields (i.e. adiabatic, collisionless, and tenuous). Nonetheless, it is important to point out that a fundamental difference exists between the highly successful single particle modeling of the main dipole plasma (the ring current), and the yet to be substantiated particle modeling of the plasma sheet plasma.

In the case of the plasma populating the main dipole, the magnetic field in which the individual particles are assumed to travel is curl-free. This means that no a priori assumptions have been made about the radiation belt current system, since, in fact, the magnetic fields produced by the ring current are a <u>second</u>

order perturbation to the main field. Since the main dipole field is produced by currents distant from the plasma, it is a simple matter to insert test particles into the field and then determine what perturbation effect they might produce.

The situation is entirely different in the plasma sheet, where the magnetic field is anything but curl-free. In fact, the plasma sheet currents change the magnetic field due to the dipole, in the first order. It is the very nature of the plasma sheet, in that the populating plasma modifies the magnetic field in which it moves, that makes the magnetotail unique and demands a self-consistent solution. In order to compute trajectories in the tail it is necessary to first specify the magnetic field. But upon specifying the field, we have automatically determined the current system to first order, which is just the curl of the field. Injecting test particles into such a field can do little more than illustrate and confirm the prescribed current system, and in some cases indicate that collective effects may be important (if electrons and ions move in such a way that charge buildup is inevitable).

In the case of the magnetotail, we have discovered the latter. The only way to gain further insight using single particles is to assume the effects of charge buildup are negligible. In addition, we can expect that the inertia of the ions dominates the motion.

Let us now examine the question concerning the current driven by the cross-tail electric field. In the following discussion, it

is very important to make the distinction between the actual magnetotail, and the simpler model which concerns us here. In the actual magnetotail the magnetic component B_z is not constant, just slowly varying, so that the associated electric field cannot be transformed away (except perhaps locally). Nonetheless, in our model the electric field can easily be "transformed away" everywhere, simply by looking at the model from a properly chosen reference frame. In this special moving frame, traveling earthward (+x) with speed E_y/B_z, there still exists magnetic field, but no electric field. The important point here is that as long as the transformation velocity is much less than the speed of light, then the magnetic field is identical in both frames. If the magnetic field is the same in both frames, then the currents producing the fields must also be the same, a direct result of the steady state Maxwell equation $\nabla \times \vec{B} = \mu_o \vec{J}$. If the currents are the same in both frames, regardless of the associated electric field, then we can only conclude that the electric field has no effect on the current, which is the same as saying the electric field drives no current. Note we are not saying that the electric field has no effect on particle motion (which it does).

Now the above discussion showing there can be no electric-driven current, coupled with the earlier analysis on particle motions with electric fields, leads to a confusing paradox. The paradox is resolved once we realize we are confusing two quantities,

namely the macroscopic current j, and the microscopic current produced by a single particle. There is no way we can expect a test particle to yield information about the macroscopic current j, without making collective assumptions and averaging over all constituent particles. Therefore, in order to compute j we need to know the velocity distribution of all the populating particles, and then add each particle's current contribution to get the corresponding macroscopic quantity. The current we get must equal the current derived from the curl of B, or else a mistake has been made. The fact that the next section, using arguments parallel to Speiser's, yields a current which depends on E_y simply illustrates that a plasma with the velocity distribution assumed cannot produce current self-consistent with the model magnetic field. Note the assumptions state that the current can be computed by multiplying the particle number density by the mean cross tail velocity. This is equivalent to assuming a monoenergetic plasma, each particle having the mean velocity, and each making the same displacement cross-tail. In other words, we have shown that a monoenergetic plasma is incapable of supporting the field configuration. Hence the paradox is only a result of the fact that we have assumed properties for the plasma that are inconsistent with the magnetic field it must produce. Even so, the single particle approach remains to be most useful for looking at perturbations or general motions.

Now we can finally try to answer the question concerning the primary current carrier. We can only attempt an answer by comparing the results for single test particles. To give a full answer it is once again necessary to know the velocity distribution of the plasma. We will just look at the ratio of current produced by single protons and electrons. The situation is complicated by the fact that the protons are of a different temperature than the electrons. To make matters worse, the individual currents also depend on the model through E_y and B_z as shown in the previous section. We expect the protons to be non-adiabatic and the electrons to be adiabatic. We will denote the current produced by an untrapped electron to be j_{ue}, and an untrapped proton j_{ui}. Restricting ourselves to cases 1,4 we get from equation (20)

$$\frac{j_{ue}}{j_{ui}} = \frac{-v_{oe} + E_y/B_z}{v_{oi} + E_y/B_z} \quad . \tag{24}$$

In the limiting case where E_y/B_z is large we get a ratio of -1, or equal and opposite current. In the case where E_y/B_z is small, we get a ratio of $-v_{oe}/v_{oi}$, which is equal to $\sqrt{m_i/m_e \cdot T_e/T_i}$. So that if $m_i/m_e \approx 1000$ and $T_e/T_i \approx 1/10$, then the ratio is about -10, or the electron current dominates.

In this section we have shown that the cross-tail electric field drives no current. Even so the literature contains references purporting to compute the cross-tail conductivity. An example is the controversial paper by Speiser (1970). In the next section Speiser's arguments are shown to apply only to a monoenergetic plasma in Case 4 untrapped motion. The argument produces the paradox discussed earlier in this section, in the sense that it predicts a current driven by the electric field. The argument is presented for completeness, and to show its extreme limitations, not to support its conclusions.

DISCUSSION OF SPEISER'S CONDUCTIVITY

In this section the development of Speiser's (1970) gyro-conductivity, in light of the new trajectory results, is discussed. It is shown that Speiser's results at best apply only to a very limited type of trajectory. All the restricting assumptions that apply to Speiser's calculations are spelled out, and generalized whenever possible. In the next section the general single particle approach is criticized with respect to the cross-tail current and is discussed in general.

In order to compute the cross-tail conductivity, it is first necessary to compute the cross-tail current. In addition, it is convenient to separate the net current into components. The components of the net current may include the curvature and

gradient drift currents, if adiabatic particles are present. Sometimes the component currents may vary with distance above the mid-plane, as has been shown for the folded figure eight orbits of Cases 3 and 6. This effect is not included in the following arguments. It is also important to distinguish between those particles which are trapped (density n_t) and those which are untrapped (density n_u).

In the following calculation, the current produced by untrapped particles is computed by dividing the net cross-tail displacement ($2\rho_o'$) by the time the particle stays in the plasma sheet (which varies according to case). To simplify matters any local currents produced by trapped orbits are ignored in the following discussion.

Now the cross-tail velocity of untrapped orbits can be computed since the net displacement a particle makes in the direction of current is $2\rho_o'$, for all cases of orbits ($2\rho_o'$ becomes $2\rho_o$ in the limiting case where $E^*<<1$. The lifetime of a particle in the sheet can vary drastically, however. Recall that the lifetime is $\pi\tau_o$ for Cases 1 and 4; it ranges from $2L/v_o$ to several bounce period for Cases 2 and 5; but it is just $2L/v_o$ for Cases 3 and 6. Therefore, the average cross-tail velocity, which is denoted by $\langle v_y \rangle$, can be expressed as

$$\langle v_y \rangle \simeq \begin{cases} \dfrac{2\rho_o'}{\pi\tau_o} & \text{Cases 1, 4} \\ \dfrac{2\rho_o'}{(2L/V_o)} & \text{all other Cases} \end{cases} \tag{18}$$

The current produced by untrapped particles with charge q can be expressed as

$$j_u = \begin{cases} \dfrac{qn_u\rho_o'}{\tau_o} \\ \dfrac{qn_u\rho_o'}{(2L/v_o)} \end{cases} \tag{19}$$

Expanding ρ_o' yields (using $2/\pi \simeq 1$),

$$j_u = qn_u \begin{cases} (v_o + \dfrac{E_y}{B_{zo}}) \\ \dfrac{mv_o}{LB_{zo}} \quad (v_o + \dfrac{E_y}{B_{zo}}) \end{cases} \tag{20}$$

If we now restrict the discussion to orbits with $E^* \gtrsim 1$, then we will insure $E_y/B_{zo} >> v_o$ so that v_o can be eliminated in the above expression as follows

$$j_u = \frac{qn_u E_y}{m} \begin{cases} \tau_o \\ \dfrac{\tau_o \rho_o}{L^*} \end{cases} \tag{21}$$

Since $L/\rho_o = L^*$ we finally get

$$j_u = \frac{qn_u E_y}{m} \begin{cases} \tau_o \\ \tau_o \\ \hline L^* \end{cases} \quad . \tag{22}$$

Therefore we may define a conductivity by taking the coefficient of E_y above,

$$\sigma_u = \frac{q^2 n_u}{m} \begin{cases} \tau_o & \text{Case 4} \\ \dfrac{\tau_o}{L^*} & \text{Cases 5 and 6 only.} \end{cases} \tag{23}$$

Clearly as the orbit becomes more adiabatic L* increases and the conductivity decreases. The conductivity is greatest for the Speiser type orbits. In fact, the above expressions are the same as Speiser's (1971) gyroconductivities, but the above expressions are limited in application only to untrapped Cases 4, 5 and 6.

CONCLUSION

A simple model of magnetic and electric fields was chosen to represent the magnetotail. The model chosen was very similar to Kan's (1973) current sheet solution. Then the equations of motion were non-dimensionalized for two simple reasons. First, the scaled equations of motion were more tractable for the computer

because all the variables became of order unity. Secondly, more physical intuition could be gained if the equations of motion were scaled by lengths and times expected to have special physical importance. In fact, one of the resulting parameters, E*, determines the amount of energization, and the other parameter, namely L*, determines the degree of adiabatic behavior. Using the dimensionless parameters (see Table 1), a systematic study was then carried out for different particle pitch and phase angles. It was found that all previous authors had merely studied orbits which fall into restricted classes, depending upon the particular values of L* and E* the author unknowingly used.

This classification into a common framework eliminated all the apparent disagreements between the various authors by showing that their conclusions were valid in the limited area of the parameter space of E* and L*, and cannot be applied to plasma sheet particle motion in general. In addition to eliminating the confusion, this study completed the picture by finding all those trajectories not previously discussed. The most important addition was probably the drift-free folded figure eight orbits demonstrating that plasma sheet particles do not drift across the tail like dipole particles do in the ring current, but nonetheless support the satellite observations of a thin current sheet imbedded in the thicker plasma sheet.

Another conclusion, which was a direct result from scaling the equations of motion, was that the maximum cross-tail displacement of untrapped particles was shown to be one gyrodiameter in the E = 0 frame. This result was then combined with the Lorentz transformation to provide a simple procedure for predicting particle energization without any further need of numerical computations.

Lastly, it is shown that the Speiser (1970) concept of gyroconductivity was inadequate because it was not self-consistent with the model field to which it was applied. In fact, the transformation argument was invoked to show the cross-tail electric field drives no current at all. The question of the primary current carrier was resolved, since the electron and ion currents were found to be equal until $E^* \gtrsim 1$, in which case the electron current dominates.

This thesis has unified several studies which concern particle motion in the tail, and has attempted to fill in the remaining gaps, at least in terms of orbit morphology. In addition, several related problems concerning the effects of the cross-tail electric field were addressed. Further improvements could be made by making refinements in the model to more closely simulate the magnetotail. For example, a model with a gradient in B_z would be very interesting. However, these improvements would likely be of a minor nature. What is really needed is a true self-consistent field plasma model, either numerical or analytical. This requires an altogether

new approach, although the single particle analysis in this thesis should remain essential as the first step in providing the physical intuition required to describe the features to be included in the next more advanced analysis.

APPENDIX A THE NUMERICAL INTEGRATION OF TRAJECTORIES

Only in recent years have computers and computing algorithms developed to the point where charged particle trajectories can be computed easily and efficiently. Much progress has been made since the laborious hand calculations of Stormer (1955). In fact, modern algorithms have taken a dramatic step forward since the early numerical work of Speiser (1965). Elementary descriptions and relative comparisons of the currently available trajectory integrators can be found in the literature discussing the numerical solutions of systems of ordinary differential equations. The most important review papers on the subject include Clark (1968) and Hull et al. (1972, 1975). Further up to date information, including complete derivations of the more classical methods, can be found in the reference text by Gear (1971). All of these references concur that even the early version of the rational function extrapolation algorithm introduced by Bulisch and Stoer (1968) is the most efficient available for trajectory integrations. In many cases the extrapolation algorithm was found to be an order of magnitude more efficient than the more classical methods which include Taylor expansions, Runge-Rutta variations, and multi-step predictor-correctors. More recently Stoer (1975, and unpublished correspondence) has introduced further improvements in the algorithm's stepsize monitor, yielding yet another order of magnitude gain in efficiency. As a result the improved Bulisch-Stoer algorithm is

the most accurate and efficient trajectory integrator available today.

In this section the improved algorithm will be discussed, and a Fortran encoding included for completeness. First consider a system of m ordinary differential equations,

$$y_1' = f_1\ (t,\ y_1,\ y_2,\ y_3,\ \ldots y_m)$$
$$y_2' = f_2\ (t,\ y_1,\ y_2,\ y_3,\ \ldots y_m)$$
$$\vdots$$
$$y_m' = f_m\ (t,\ y_1,\ y_2,\ y_3,\ \ldots y_m).$$

With no loss of generality we can let y be the vector $y = (y_1,\ y_2,\ y_3,\ \ldots y_m)$. Then we only need to examine the solution of the single vector equation

$$y' = f(t,y),$$

subject to the initial condition

$$y(t_o) = y_o.$$

For a particle trajectory y is just the vector $(x,\ y,\ z,\ v_x,\ v_y,\ v_z)$ in six-space, and t represents time. Let us assume this first order differential equation is integrable in principle, and denote

the actual solution by y(t), even though in actuality we will only be able to approximate y(t) numerically. Now to proceed with the formulation, we decide we want to solve for an approximation to y(t) for all t in some solution interval $L = [t_i, t_f]$. But first we try to approximate y(t) over some smaller interval $H \subset L$. We will call H the stepsize, and we will cover the interval L by using a sequence of H's, which we will vary to make the solution proceed as efficiently as possible. In order to approximate y(t) over H, it will be necessary to subdivide H into a special sequence of smaller substeps by

$$h_i = \frac{H}{n_i} \quad .$$

The sequence of h_i is clearly a function of both the stepsize H and a special sequence of natural numbers, which were chosen by Bulisch and Stoer (1964) to minimize the number of calculations. It turns out that the optimum sequence of n_i is

$$n_i \in \{1, 2, 3, 4, 6, 8, 12, 16, \ldots\} \quad .$$

We can now apply the modified midpoint rule to each pair (h_i, n_i) or just (h, n) and get an approximation to y(t) which we will write as $\eta(t, h)$. The rule states,

$$\eta_o = y_o$$

$$\eta_i = \eta_o + \frac{h}{2} f(t_o, \eta_o)$$

For $i = 1, 2, 3, \ldots 2n-1$, $t_i = t_o + i\frac{h}{2}$

$$\eta_{i+1} = \eta_{i-1} + hf(t_i, \eta_i)$$

$$\eta(t, h) = \tfrac{1}{2}\{\eta_{2n} + \eta_{2n-1} + \frac{h}{2}\}$$

so that the sequence of $\eta(t, h_o)$, $\eta(t, h_1)$, $\eta(t, h_2)\ldots$ represents a sequence of increasingly better approximations to $y(x)$. Now we form a tableau of approximations T_{ik}, in which the first column of the tableau T_{1k} is equal to the sequence $\eta(t, h_k)$. The other elements of the tableau are computed from a recursion relationship derived by Bulisch and Stoer (1964). They found the recursion relationship by extrapolating an arbitrary rational function of the form

$$\hat{T}_{ik}(h) = \frac{C_{io} + C_{i1}h^2 + C_{i2}h^4 + \ldots C_{i\mu}h^{2\mu}}{d_{io} + d_{i1}h^2 + C_{i2}h^4 + \ldots d_{i\nu}h^{2\nu}}$$

where $\mu = k/2$, $\nu = k - \mu$. The extrapolation is performed under the assumption that

$$T_{ik} = \lim_{h \to o} \hat{T}_{ik}(h)$$

and that

$$\hat{T}_{ik}(h_j) = \eta(t, h_j), \quad j = i, i-1, \ldots i-k.$$

The resulting recursion relationship is

$$T_{ik} = T_{i+1,\,k-1} + \frac{(T_{i+1,\,k-1} - T_{i,\,k-1})}{(\frac{h_i}{h_{i+k}})^2 \left(1 - \frac{(T_{k+1,\,k-1} - T_{i,\,k-1})}{(T_{i+1,\,k-1} - T_{i+1,\,k-2})}\right) - 1}$$

Now each successive T_{ik} represents a better approximation to $y(x)$. We need a criterion to decide when to stop computing the T_{ik}. It is important to realize that each consecutive row, specified by the index k, of the tableau represents an increase in the order of the approximating rational function. It is in this way that the algorithm is said to be a 'variable order' method, that is the order is increased automatically simply by computing the next row of the tableau. This is very efficient because it is not necessary to backtrack or repeat calculations before increasing the order. To complicate matters, though, the order is not necessarily the most economical thing to do. In some cases it would be better to decrease the stepsize H, so that fewer tableau entries are needed to fulfill the error constraint. To determine the optimum strategy, it is necessary to know the cost of the alternatives and the

accuracy required. Let us assume that the first H is given. Then the relative error for each T_{ik} is defined as

$$\varepsilon_{ik} = |T_{ik} - y(x)|$$

It can be shown that ε_{ik} is alternately given by

$$\varepsilon_{ik} = \left|\frac{T_{ik} - T_{i-1,\,k}}{S}\right| \left(\frac{\eta_{i-k-1}}{n_i}\right)^2$$

where $S = \max |y(z)|$, $z \varepsilon H$. Hence if we specify the maximum allowable error ε, we only need to compute T_{ik} until ε_{ik} specified above is less than ε. All that is left is to compute the next suggested stepsize H', based on the optimum strategy method. The algorithm is set up so that it will always integrate over H if it can make $\varepsilon_{ik} < \varepsilon$. It then suggests a new step H', based on a strategy which is a function of ε, ε_{ik}, T_{ik}, and the cost of function evaluations. In the original algorithm Bulisch and Stoer (1968) suggested a stepsize monitor which depended only on the maximum order k_{max} of the T_{ik}'s, computed to make $\varepsilon_{ik} < \varepsilon$. They suggested that if it was necessary to compute the T_{ik} for $k_{max} \geq 7$, then H was probably too large. On the other hand, if $k_{max} < 7$, then H was too small. They suggested a monitor of

$$H' = H \cdot .9 \cdot (.6)^{m-7} \qquad m > 7$$

$$H' = H \cdot 1.5 \qquad m < 7.$$

Later research by Stoer (1975, private communication) showed that this monitor was far too conservative. Using an optimum strategy argument, Stoer suggested the improved monitor:

$$H' = H/\mu,$$

where

$$f_{ik} = (n_i n_{i-1} \ldots n_{i-k})^2$$

$$\alpha = \sqrt[2\ell+3]{\varepsilon \cdot f_{\ell\ell}}$$

are needed to compute

$$\mu = \begin{cases} \frac{1}{\alpha}\sqrt[2i+1]{\frac{|T_{j,\,j-1} - T_{j-1,j-1}|}{S}\, f_{j-1,\,j-1}} & \text{if } j \geq \ell \\ \frac{1}{\alpha}\sqrt[2\ell+3]{\frac{|T_{j,\ell} - T_{j-1,\,\ell}|}{S}\, f_{j-1,\,\ell}} & \text{if } j > \ell \end{cases}$$

This monitor showed another order of magnitude gain in efficiency for all trajectories that required stepsize changes. It is this improved algorithm that is included in the following Fortran encoding.

APPENDIX B FORTRAN ENCODING

The following Fortran encoding contains a controlling program "SUBROUTINE PLASMA" and several subordinate subroutines. The controlling program is interactive in time sharing and allows the user to run the program by answering simple questions concerning the field model and the particles' initial conditions. The proper magnetic field model must be stored in "SUBROUTINE FIELD." Any electric and magnetic field, even a dipole, can be used. The equations of motion are included in "SUBROUTINE F." The algorithm for rational function extrapolation, which is the core of the program, is in "SUBROUTINE SABER." The plotting subroutines, which are easily modified, are included in "SUBROUTINE PLOT 3" and "SUBROUTINE INFO." The capability of storing the data is included, and if the user answers "yes" to the data save question, he will find the data stored in file #6. The file number is easily changed to match the host computer.

```
      SUBROUTINE PLASMA
      DOUBLE PRECISION X,H,HMIN, HMAX, EPS, Q, M, QM, ENERGY, ALPHA, PHI
      DOUBLE PRECISION Y(30), DY(30), YMAX(30), ERROR(30)
      DOUBLE PRECISION B(3), V(3), VP(3),EL(3)
      INTEGER PLTIND, DFLAG
      LOGICAL LOGG
      DIMENSION XPLOT(1000), YPLOT(1000), ZPLOT(1000), VXPRINT(1000)
      DIMENSION VYPRINT(1000), VZPRINT(1000), TPRINT(1000)
C*****************************************************************************
C*     SUBROUTINE PLASMA IS THE MAIN CONTROLLING PROGRAM FOR THIS CURRENT  *
C*     SHEET SOLUTION ROUTINE. THE SUBROUTINE IS INTERACTIVE IN THE TIME   *
C*     SHARE SYSTEM AND AS SUCH IS SELF EXPLANATORY. CARE MUST BE TAKEN    *
C*     TO INSURE THAT THE UNITS IN SUBROUTINE FIELD MATCH THOSE SPECIFIED  *
C*     FOR QM.                                                             *
C*****************************************************************************
      DIMENSION A(2),P(2),E(2)
      COMMON QM,A,P,E,VXPRINT,VYPRINT,VZPRINT,H,HMAX,EPS,MAXORD,ELFY,XLMDA,ZLMDA
      PRINT: "CHARGED PARTICLE TRAJECTORY PROGRAM NO. 1"
      PRINT: "PLASMA SHEET MODEL"
      PRINT: " "
      PRINT: "ENTER 0 FOR DIMENSIONLESS UNITS"
      PRINT: "ENTER 1 FOR MKS UNITS (PROTON)"
      PRINT: "ENTER 2 FOR MKS UNITS (ELECTRON)"
      PRINT: "ENTER 3 FOR ARBITRARY Q/M"
      READ: DFLAG
      DFLAG = DFLAG + 1
      GO TO (10, 20, 30, 40),DFLAG
   10 CONTINUE
      QM = 1.0D0
      M=1.D0
      GO TO 50
   20 CONTINUE
      QM = .9578969D08
      M=1.672614D-27
      GO TO 50
   30 CONTINUE
      QM = -.1758803D12
      M=9.109558D-31
      GO TO 50
   40 CONTINUE
      PRINT: "ENTER CHARGE AND MASS"
      PRINT: "Q =  ?, M =  ?"
      READ: Q,M
      QM = Q/M
   50 CONTINUE
      PRINT: "ENTER 1 TO ENTER INITIAL VELOCITIES"
      PRINT: "ENTER 0 TO ENTER INITIAL ENERGY, PITCH, PHASE"
      READ: DFLAG
      DFLAG = DFLAG + 1
      PRINT: "X =  ?, Y =  ?, Z =  ?"
      READ: Y(1), Y(2), Y(3)
      X=0.0
      XPLOT(1) = Y(1)
      YPLOT(1) = Y(2)
```

```
560 ZPLOT(1) = Y(3)
570 PRINT:"E(Y)=?,ZLAMDA=?"
580 READ:ELFY,ZLMDA
590 CALL FIELD (X,Y,B,EL)
600 GO TO (70,60),DFLAG
610 60 CONTINUE
620 PRINT: "ENTER INITIAL VELOCITIES"
630 PRINT: "VX =  ?, VY =  ?, VZ =  ?"
640 READ: Y(4), Y(5), Y(6)
650 V(1) = Y(4)
660 V(2) = Y(5)
670 V(3) = Y(6)
680 LOGG=.FALSE.
690 CALL PITCH (V,VP,ENERGY,ALPHA,PHI,B,M,LOGG)
700 A(1)=ALPHA
710 P(1)=PHI
720 E(1)=ENERGY
730 PRINT:" "
740 PRINT:"ENERGY=",E(1)
750 PRINT:"PITCH ANGLE=",A(1);PRINT:"PHASE ANGLE=",P(1);PRINT:" "
760 GO TO 80
770 70 CONTINUE
780 ENERGY=.5
790 E(1)=.5
800 PRINT: "ENTER INITIAL PITCH, PHASE"
810 PRINT: "ALPHA =  ?, PHI =  ?"
820 READ: ALPHA, PHI
830 A(1)=ALPHA
840 P(1)=PHI
850 LOGG=.TRUE.
860 CALL PITCH (V,VP,ENERGY,ALPHA,PHI,B,M,LOGG)
870 PRINT:" "
880 PRINT:"VX=", V(1);PRINT:"VY=", V(2);PRINT:"VZ=", V(3);PRINT:" "
890 Y(4) = V(1)
900 Y(5) = V(2)
910 Y(6) = V(3)
920 80 CONTINUE
930 TPRINT(1) = X
940 VXPRINT(1) = Y(4)
950 VYPRINT(1) = Y(5)
960 VZPRINT(1) = Y(6)
970 PRINT: "COMPUTE TRAJECTORY FOR HOW MANY POINTS?"
980 READ: NPTS
990 IF(NPTS.LE.0)NPTS=50
1000 PRINT: "MAXIMUM STEP SIZE ALLOWED?"
1010 READ: HMAX
1020 IF(HMAX.LE.1.D-8)HMAX=100.D0
1030 PRINT: "FIRST GUESS STEP SIZE"
1040 READ: H
1050 IF(H.LE.1.D-8)H=1.D0
1060 PRINT: "MAXIMUM ALLOWABLE SINGLE STEP ERROR?"
1070 READ: EPS
1080 IF(EPS.LE.1.D-15)EPS=1E-6
1090 MAXORD=6
```

```
1100 PRINT: "DO YOU WANT THE DATA SAVED?"
1110 PRINT: "ENTER 0 IF YES"
1120 PRINT: "ENTER 1 IF NO"
1130 READ: DFLAG
1140 DFLAG = DFLAG + 1
1150 GO TO (90,100),DFLAG
1160 90 CONTINUE
1170 IO=06
1180 100 CONTINUE
1190 JSTART = 1
1200 MAXPTS = 2*MAXORD + 2
1210 N = 6
1220 HMIN = H*1.D-8
1230 MF = 0
1240 DO 110 L = 1,30
1250 ERROR(L) = 1.D0
1260 110 CONTINUE
1270 DO 120 L = 2,NPTS
1280 CALL SABER(N,X,Y,H,EPS,ERROR)
1290 XPLOT(L) = Y(1)
1300 YPLOT(L) = Y(2)
1310 ZPLOT(L) = Y(3)
1320 VXPRINT(L) = Y(4)
1330 VYPRINT(L) = Y(5)
1340 VZPRINT(L) = Y(6)
1350 TPRINT(L) = X
1360 IF(ABS(ZPLOT(L)).GT.ABS(ZPLOT(1)).AND.L.GT.50)GO TO 125
1370 IF (H.GT.HMAX) H = HMAX
1380 120 CONTINUE
1390 125 CONTINUE
1400 NPTS=L
1410 PRINT:"T=",TPRINT(L)
1420 CALL FIELD(X,Y,B,EL)
1430 V(1)=Y(4)
1440 V(2)=Y(5)
1450 V(3)=Y(6)
1460 LOGG = .FALSE.
1470 CALL PITCH(V,VP,ENERGY,ALPHA,PHI,B,M,LOGG)
1480 A(2)=ALPHA
1490 P(2)=PHI
1500 E(2)=ENERGY
1510 PRINT:" ";PRINT:"FINAL ENERGY=",E(2);PRINT:"FINAL PITCH ANGLE=",A(2)
1520 PRINT:"FINAL PHASE ANGLE=",P(2);PRINT:" "
1530 140 CONTINUE
1540 PRINT: "PLOTTING OPTIONS:"
1550 PRINT: "X-Z GRAPH ENTER 1"
1560 PRINT: "Y-Z GRAPH ENTER 2"
1570 PRINT: "X-Y GRAPH ENTER 3"
1580 PRINT: "ALL THREE VIEWS ENTER 4"
1590 PRINT: "ALL FOUR PLOTS ENTER 5"
1600 PRINT: "NO PLOT ENTER 0"
1610 READ: PLTIND
1620 IF (PLTIND .EQ.0) GO TO 150
1630 IF (PLTIND .EQ.5) GO TO 160
```

```
      CALL PLOT3(NPTS, XPLOT, YPLOT, ZPLOT, PLTIND)
      GO TO 140
  160 CONTINUE
      DO 170 L = 1,4
      LL=L
      CALL PLOT3(NPTS, XPLOT, YPLOT, ZPLOT, LL)
  170 CONTINUE
  150 CONTINUE
      IF (DFLAG .EQ.2) GO TO 180
      WRITE(IO) M,NPTS,(TPRINT(L), XPLOT(L), YPLOT(L), ZPLOT(L),
     & VXPRINT(L), VYPRINT(L), VZPRINT(L), L = 1,NPTS)
      PRINT: "DATA SAVED IN", IO
  180 CONTINUE
      STOP
      END
      SUBROUTINE PITCH(V,VP,E,ALPHA,PHI,B,M,MFLAG)
      LOGICAL MFLAG
      DOUBLE PRECISION V(3),VP(3),B(3),A(3,3)
      DOUBLE PRECISION M,ALPHA,PHI,E,BX,BY,BZ,BXZ,BXYZ,BB,VV,ARG,CONV
      CONV=180.D0/3.14159265358979323384D0
C*****************************************************************************
C*     THIS SUBROUTINE COMPUTES AN ORTHOGONAL TRANSFORMATION MATRIX          *
C*   WHICH TRANSFORMS VECTORS IN THE EARTH CENTERED FRAME TO THE             *
C*   GUIDING CENTER SYSTEM (AND BACK AGAIN) , IN AN ARBITRARY MAGNETIC       *
C*   FIELD.THE PARAMETERS USED HAVE THE FOLLOWING MEANING:                   *
C*           V=VELOCITY VECTOR IN THE EARTH SYSTEM                           *
C*           VP=VELOCITY VECTOR IN THE GUIDING CENTER SYSTEM                 *
C*           E=TOTAL ENERGY IN THE EARTH SYSTEM                              *
C*           ALPHA=THE PITCH ANGLE IN DEGREES 0<ALPHA<180                    *
C*           PHI=THE PHASE ANGLE IN DEGREES -180<PHI<180                     *
C*           B=MAGNETIC FIELD VECTOR                                         *
C*           M=THE MASS OF THE PARTICLE                                      *
C*           MFLAG=THE METHOD FLAG, WHICH CAN BE;                            *
C*                 "F"=GIVEN V IN EARTH SYSTEM FIND ALPHA,PHI,E              *
C*                 "T"=GIVEN ALPHA,PHI,E, FIND V                             *
C*****************************************************************************
      BX=B(1)
      BY=B(2)
      BZ=B(3)
      BXZ=BX**2+BZ**2
      BXYZ=DSQRT((BX**2)*(BY**2)+BXZ**2+(BZ**2)*(BY**2))
      BB=DSQRT(BY**2+BXZ)
      A(1,1)=BZ/DSQRT(BXZ)
      A(1,2)=-BY*BX/BXYZ
      A(1,3)=BX/BB
      A(2,1)=0.D0
      A(2,2)=BXZ/BXYZ
      A(2,3)=BY/BB
      A(3,1)=-BX/DSQRT(BXZ)
      A(3,2)=-BY*BZ/BXYZ
      A(3,3)=BZ/BB
      IF(DABS(BX).GT.0.D0.OR.DABS(BZ).GT.0.D0)GO TO 5
      DO 1 I=1,3
      DO 1 J=1,3
```

```
      A(I,J)=0.D0
    1 CONTINUE
      A(1,1)=1.D0
      A(2,3)=1.D0
      A(3,2)=-1.D0
      IF(BY.LT.0.D0) A(2,3)=-1.D0
      IF(BY.LT.0.D0)A(3,2)=1.D0
    5 CONTINUE
      IF (.NOT.MFLAG) GO TO 10
C*****************************************************************************
C*     COMPUTE THE VELOCITY IN THE PRIMED SYSTEM                             *
C*****************************************************************************
      VV=DSQRT(2.D0*E/M)
      PHI=PHI/CONV
      ALPHA=ALPHA/CONV
      VP(1)=-DSIN(PHI)*VV*DSIN(ALPHA)
      VP(2)=DCOS(PHI)*VV*DSIN(ALPHA)
      VP(3)=VV*DCOS(ALPHA)
C*****************************************************************************
C*     TRANSFORM THE VELOCITIES INTO THE EARTH SYSTEM                        *
C*****************************************************************************
      DO 15 I=1,3
      V(I)=0.D0
   15 CONTINUE
      DO 20 I=1,3
      DO 20 J=1,3
      V(I)=V(I)+VP(J)*A(I,J)
   20 CONTINUE
      RETURN
   10 CONTINUE
C*****************************************************************************
C*     TRANSFORM THE VELOCITIES INTO THE PRIMED(G.C.) SYSTEM                 *
C*****************************************************************************
      VV=DSQRT(V(1)**2+V(2)**2+V(3)**2)
      DO 25 I=1,3
      VP(I)=0.D0
   25 CONTINUE
      DO 30 I=1,3
      DO 30 J=1,3
      VP(I)=VP(I)+V(J)*A(J,I)
   30 CONTINUE
      ALPHA=90.D0
      IF(DABS(VP(3)).LT.1D-19)GO TO 35
      ALPHA=CONV*DATAN(DSQRT(VP(1)**2+VP(2)**2)/VP(3))
      IF(DABS(VP(1))+DABS(VP(2))/VV.LT.1D-7.AND.VP(3).LT.0D0)ALPHA=180.D0
      IF(ALPHA.LT.0.D0)ALPHA=180+ALPHA
   35 CONTINUE
      IF(DABS(VP(1)).LT.1.D-7.AND.VP(2).GT.0.D0)PHI=0.D0
      IF(DABS(VP(2))/VV.LT.1.D-7.AND.VP(1).GT.0.D0)PHI=-90.D0
      IF(DABS(VP(1))/VV.LT.1.D-7.AND.VP(2).LE.0.D0)PHI=180.D0
      IF(DABS(VP(2))/VV.LT.1.D-7.AND.VP(1).LT.0.D0)PHI=90.D0
      IF(VP(1).GE.0.D0.AND.VP(2).GT.0.D0)PHI=CONV*DATAN(-VP(1)/VP(2))
      IF(VP(1).LT.0.D0.AND.VP(2).GT.0.D0)PHI=CONV*DATAN(-VP(1)/VP(2))
      IF(VP(1).LT.0.D0.AND.VP(2).LT.0.D0)PHI=CONV*DATAN(-VP(1)/VP(2))+180.D0
```

```
2720 IF(VP(1).GT.0.D0.AND.VP(2).LT.0.D0)PHI=CONV*DATAN(-VP(1)/VP(2))-180.D0
2730 E=M*(VV**2)/2.D0
2740 RETURN
2750 END
2760 SUBROUTINE F(X,Y,DY)
2770 ************************************************************************
2780 *     SUBROUTINE F IS USED BY SUBROUTINE SABER TO COMPUTE THE DERIVATIVES *
2790 *     FROM THE SYSTEM OF DIFFERNTIAL EQUATIONS THAT CAN BE OBTAINED FROM  *
2800 *     THE LORENTZ FORCE EQUATION F=Q/M(VxB+E).                            *
2810 ************************************************************************
2820 DOUBLE PRECISION Y(30), DY(30), B(3), E(3)
2830 DOUBLE PRECISION QM,X
2840 COMMON QM
2850 CALL FIELD (X,Y,B,E)
2860 DY(1)=Y(4)
2870 DY(2)=Y(5)
2880 DY(3)=Y(6)
2890 DY(4)=(Y(5)*B(3)-Y(6)*B(2)+E(1))*QM
2900 DY(5)=(Y(6)*B(1)-Y(4)*B(3)+E(2))*QM
2910 DY(6)=(Y(4)*B(2)-Y(5)*B(1)+E(3))*QM
2920 RETURN
2930 END
2940 SUBROUTINE FIELD (X,Y,B,E)
2950 ************************************************************************
2960 *     SUBROUTINE FIELD COMPUTES THE ELECTRIC AND MAGNETIC FIELDS FOR A    *
2970 *     MODEL CURRENT SHEET.                                                *
2980 ************************************************************************
2990 DOUBLE PRECISION Y(30), B(3), E(3)
3000 DOUBLE PRECISION X, BX0, BZ0, XL, Z, ZM,ZL
3010 DIMENSION A(2),P(2),EE(2)
3020 DOUBLE PRECISION QM,H,HM,EPS
3030 COMMON QM,A,P,EE,VX(1000),VY(1000),VZ(1000),H,HM,EPS,MAXORD,ELFY,XLMDA,ZLMDA
3040 BX0=-1.D0
3050 BZ0=1.D0
3060 XLMDA=1.
3070 XL=XLMDA
3080 ZL=ZLMDA
3090 B(1)=BX0*DTANH(Y(3)/ZL)
3100 B(3)=BZ0
3110 B(2)=0.D0
3120 E(1)=0.D0
3130 E(2)=ELFY
3140 E(3)=0.D0
3150 RETURN
3160 END
3170 SUBROUTINE PLOT3(M,X,Y,Z,PLTIND)
3180 REAL X(M),Y(M),Z(M)
3190 INTEGER PLTIND
3200 CALL PLOTST
3210 N=M
3220 GO TO (10,20,30,40),PLTIND
3230 10 CONTINUE
3240 CALL SCALE(X,10.,N,1,10.)
3250 CALL SCALE(Z,10.,N,1,10.)
```

```
3260 CALL AXIS(0.,0.,"X-AXIS",-6,10.,0.,X(N+1),X(N+2),10.)
3270 CALL AXIS(0.,0.,"Z-AXIS",6,10.,90.,Z(N+1),Z(N+2),10.)
3280 CALL LINE(X,Z,N,1,1,1)
3290 GO TO 50
3300 20 CONTINUE
3310 CALL SCALE(Y,10.,N,1,10.)
3320 CALL SCALE(Z,10.,N,1,10.)
3330 CALL AXIS(0.,0.,"Y-AXIS",-6,10.,0.,Y(N+1),Y(N+2),10.)
3340 CALL AXIS(0.,0.,"Z-AXIS",6,10.,90.,Z(N+1),Z(N+2),10.)
3350 CALL LINE(Y,Z,N,1,1,2)
3360 GO TO 50
3370 30 CONTINUE
3380 CALL SCALE(X,10.,N,1,10.)
3390 CALL SCALE(Y,10.,N,1,10.)
3400 CALL AXIS(0.,0.,"X-AXIS",-6,10.,0.,X(N+1),X(N+2),10.)
3410 CALL AXIS(0.,0.,"Y-AXIS",6,10.,90.,Y(N+1),Y(N+2),10.)
3420 CALL LINE(X,Y,N,1,1,3)
3430 GO TO 50
3440 40 CONTINUE
3450 CALL SCALE(X,4.8,N,1,10.)
3460 CALL SCALE(Y,4.8,N,1,10.)
3470 CALL SCALE(Z,4.8,N,1,10.)
3480 CALL AXIS(0.,0.,"X-AXIS",-6,4.8,0.,X(N+1),X(N+2),10.)
3490 CALL AXIS(0.,0.,"Z-AXIS",6,4.8,90.,Z(N+1),Z(N+2),10.)
3500 CALL LINE(X,Z,N,1,1,1)
3510 CALL PLOT(0.,5.2,23)
3520 CALL AXIS(0.,0.,"X-AXIS",-6,4.8,0.,X(N+1),X(N+2),10.)
3530 CALL AXIS(0.,0.,"Y-AXIS",6,4.8,90.,Y(N+1),Y(N+2),10.)
3540 CALL LINE(X,Y,N,1,1,3)
3550 CALL PLOT(0.,-5.2,23)
3560 CALL PLOT(5.2,0.,23)
3570 CALL AXIS(0.,0.,"Y-AXIS",-6,4.8,0.,Y(N+1),Y(N+2),10.)
3580 CALL AXIS(0.,0.,"Z-AXIS",6,4.8,90.,Z(N+1),Z(N+2),10.)
3590 CALL LINE(Y,Z,N,1,1,4)
3600 CALL PLOT(-5.,0.,23)
3610 CALL INFO(N,X,Y,Z)
3620 50 CONTINUE
3630 CALL PLOT(20.,0.,-3)
3640 RETURN
3650 END
3660 SUBROUTINE INFO(N, XX, YY, ZZ)
3670 DIMENSION XX(N), YY(N), ZZ(N)
3680 DIMENSION A(2), P(2), E(2)
3690 DOUBLE PRECISION QM,H,HM,EPS
3700 COMMON QM, A, P, E, VX(1000), VY(1000), VZ(1000), H, HM, EPS, MAXORD
3710 ************************************************************************
3720 *  SUBROUTINE INFO IS REPONSIBLE FOR PLOTTING THE TRAJECTORY           *
3730 *  INFORMATION ON THE 3-PROJECTION PLOT PRODUCED BY SUBROUTINE         *
3740 *  PLOT3. THE PARAMETERS HAVE THE SAME MEANING AS IN THE CALLING       *
3750 *  PROGRAMS                                                            *
3760 ************************************************************************
3770 NN = N
3780 CALL PLOT (4.8, 5.0, 23)
3790 Y = 0.0
```

```
3800 X=0.0
3810 HIDTH = .18
3820 WIDTH=6.*HIDTH/7.
3830 SPACE = HIDTH*1.5
3840 Y = Y + 3.*SPACE
3850 CALL SYMBOL (X, Y, HIDTH," MAXORD=", 0.,8)
3860 X=X+8.*WIDTH
3870 XORD = MAXORD
3880 CALL NUMBER (X, Y, HIDTH, XORD, 0.0, -1)
3890 X=X+4.*WIDTH
3900 CALL SYMBOL (X, Y, HIDTH, " NPTS=", 0.0, 6)
3910 X=X+6.*WIDTH
3920 XNPTS = NN
3930 CALL NUMBER (X, Y, HIDTH, XNPTS, 0.0, -1)
3940 Y = Y + SPACE
3950 X=0.0
3960 CALL SYMBOL (X, Y, HIDTH, " H=", 0.0, 3)
3970 X=X+3.*WIDTH
3980 XH=H
3990 CALL EFORM (X, Y, HIDTH, XH, 0.0, 4, 3)
4000 X=X+10.*WIDTH
4010 CALL SYMBOL (X, Y, HIDTH, " HMAX=", 0.0, 6)
4020 X=X+6.*WIDTH
4030 XHM=HM
4040 CALL EFORM (X, Y, HIDTH, XHM, 0.0, 4, 3)
4050 X=X+10.*WIDTH
4060 Y = Y + SPACE
4070 X=0.0
4080 CALL SYMBOL (X, Y, HIDTH, " EPS=", 0.0, 5)
4090 X=X+5.*WIDTH
4100 XEPS=EPS
4110 CALL EFORM (X, Y, HIDTH, XEPS, 0.0, 4, 3)
4120 Y = Y + SPACE
4130 X=0.
4140 CALL SYMBOL (X, Y, HIDTH, "PLOT PARAMETERS", 0.0, 15)
4150 Y = Y + SPACE
4160 CALL SYMBOL (X, Y, HIDTH, " PITCH=", 0.0, 7)
4170 X=X+7.*WIDTH
4180 CALL NUMBER (X, Y, HIDTH, A(2), 0.0, 1)
4190 X=X+6.*WIDTH
4200 CALL SYMBOL (X, Y, HIDTH, " PHASE=", 0.0, 7)
4210 X=X+7.*WIDTH
4220 CALL NUMBER (X, Y, HIDTH, P(2), 0.0, 1)
4230 Y = Y + SPACE
4240 X = 0.0
4250 CALL SYMBOL (X, Y, HIDTH, " ENERGY=", 0.0, 8)
4260 X=X+8.*WIDTH
4270 CALL EFORM (X, Y, HIDTH, E(2), 0.0, 4, 3)
4280 X=X+10.*WIDTH
4290 CALL SYMBOL(X, Y, HIDTH, " VZ=", 0.0, 4)
4300 X=X+4.*WIDTH
4310 CALL EFORM(X, Y, HIDTH, VZ(NN), 0.0, 4, 3)
4320 Y = Y + SPACE
4330 X=0.0
```

```
4340 CALL SYMBOL (0.0, Y, HIDTH, " VX=", 0.0, 4)
4350 X=X+4.*WIDTH
4360 CALL EFORM (X, Y, HIDTH, VX(NN), 0.0, 4, 3)
4370 X=X+10.*WIDTH
4380 CALL SYMBOL (X, Y, HIDTH, " VY=", 0.0, 4)
4390 X=X+4.*WIDTH
4400 CALL EFORM (X, Y, HIDTH, VY(NN), 0.0, 4, 3)
4410 Y = Y + SPACE
4420 X=0.0
4430 CALL SYMBOL (0.0, Y, HIDTH, " X=", 0.0, 3)
4440 X=X+3.*WIDTH
4450 CALL EFORM (X, Y, HIDTH, XX(NN), 0.0, 3, 2)
4460 X=X+9.*WIDTH
4470 CALL SYMBOL (X, Y, HIDTH, " Y=", 0.0, 3)
4480 X=X+3.*WIDTH
4490 CALL EFORM (X, Y, HIDTH, YY(NN), 0.0, 3, 2)
4500 X=X+9.*WIDTH
4510 CALL SYMBOL (X, Y, HIDTH, " Z=", 0.0, 3)
4520 X=X+3.*WIDTH
4530 CALL EFORM (X, Y, HIDTH, ZZ(NN), 0.0, 3, 2)
4540 Y = Y + SPACE
4550 X=0.0
4560 CALL SYMBOL (0.0, Y, HIDTH, "FINAL VALUES", 0.0, 12)
4570 Y = Y + SPACE
4580 CALL SYMBOL (0.0, Y, HIDTH, " PITCH=", 0.0, 7)
4590 X=X+7.*WIDTH
4600 CALL NUMBER (X, Y, HIDTH, A(1), 0.0, 1)
4610 X=X+6.*WIDTH
4620 CALL SYMBOL (X, Y, HIDTH, " PHASE=", 0.0, 7)
4630 X=X+7.*WIDTH
4640 CALL NUMBER (X, Y, HIDTH, P(1), 0.0, 1)
4650 Y = Y + SPACE
4660 X=0.0
4670 CALL SYMBOL (X, Y, HIDTH, " ENERGY=", 0.0, 8)
4680 X=X+8.*WIDTH
4690 CALL EFORM (X, Y, HIDTH, E(1), 0.0, 4, 3)
4700 X=X+10.*WIDTH
4710 CALL SYMBOL(X, Y, HIDTH, " VZ=",0.0, 4)
4720 X=X+4.*WIDTH
4730 CALL EFORM(X, Y, HIDTH, VZ(1), 0.0, 4, 3)
4740 X=0.0
4750 Y = Y + SPACE
4760 CALL SYMBOL (0.0, Y, HIDTH, " VX=", 0.0, 4)
4770 X=X+4.*WIDTH
4780 CALL EFORM (X, Y, HIDTH, VX(1), 0.0, 4, 3)
4790 X=X+10.*WIDTH
4800 CALL SYMBOL (X, Y, HIDTH, " VY=", 0.0, 4)
4810 X=X+4.*WIDTH
4820 CALL EFORM (X, Y, HIDTH, VY(1), 0.0, 4, 3)
4830 X=X+10.*WIDTH
4840 Y = Y + SPACE
4850 X=0.0
4860 CALL SYMBOL (0.0, Y, HIDTH, " X=", 0.0, 3)
4870 X=X+3.*WIDTH
```

```
4880 CALL EFORM (X, Y, HIDTH, XX(1), 0.0, 3, 2)
4890 X=X+9.*WIDTH
4900 CALL SYMBOL (X, Y, HIDTH, " Y=", 0.0, 3)
4910 X=X+3.*WIDTH
4920 CALL EFORM (X, Y, HIDTH, YY(1), 0.0, 3, 2)
4930 X=X+9.*WIDTH
4940 CALL SYMBOL (X, Y, HIDTH, " Z=", 0.0, 3)
4950 X=X+3.*WIDTH
4960 CALL EFORM (X, Y, HIDTH, ZZ(1), 0.0, 3, 2)
4970 Y = Y + SPACE
4980 CALL SYMBOL (0.0, Y, HIDTH, "INITIAL VALUES", 0.0, 14)
4990 Y = Y + SPACE
5000 CALL SYMBOL (0.0, Y, HIDTH, "PARTICLE TRAJECTORY PLOT", 0.0, 24)
5010 CALL PLOT (-4.8, -5.0, 23)
5020 RETURN
5030 END
5040 SUBROUTINE SABER(N,X,Y,H,EPS,S)
5050 DOUBLE PRECISION Y(30),YA(30),YL(30),YM(30),DY(30),DZ(30),DT(30,7)
5060 DOUBLE PRECISION D(7),S(30),X,XN,H,G,B,B1,U,V,C,TA,W
5070 DIMENSION EP(4)
5080 LOGICAL KONV,BO,KL,GR
5090 DATA EP/0.4E-1,0.16E-2,0.64E-4,0.256E-5/
5100 JTI=0
5110 FY=1.
5120 ETA=DABS(EPS)
5130 IF (ETA.LT.1.E-9) ETA=1.E-9
5140 DO 100 I=1,N
5150 100 YA(I)=Y(I)
5160 CALL F(X,Y,DZ)
5170 10 XN=X+H
5180 BO=.F.
5190 DO 110 I=1,N
5200 110 S(I)=0.
5210 M=1
5220 JR=2
5230 JS=3
5240 DO 260 J=1,10
5250 IF(.NOT.BO)GO TO 200
5260 D(2)=1.777777777777778
5270 D(4)=7.111111111111111
5280 D(6)=28.44444444444444
5290 GO TO 201
5300 200 D(2)=2.25
5310 D(4)=9.
5320 D(6)=36.
5330 201 IF(J.LE.7)GO TO 202
5340 L=7
5350 D(7)=64.
5360 GO TO 203
5370 202 L=J
5380 D(L)=M*M
5390 203 KONV=L.GT.3
5400 M=M+M
5410 G=H/FLOAT(M)
```

```
5420 B=G+G
5430 M=M-1
5440 DO 210 I=1,N
5450 YL(I)=YA(I)
5460 210 YM(I)=YA(I)+G*DZ(I)
5470 DO 220 K=1,M
KPP=K
5480 CALL F(X+FLOAT(KPP)*G,YM,DY)
5490 DO 220 I=1,N
5500 U=YL(I)+B*DY(I)
5510 YL(I)=YM(I)
5520 YM(I)=U
5530 U=DABS(U)
5540 IF(U.GT.S(I))S(I)=U
5550 220 CONTINUE
5560 CALL F(XN,YM,DY)
5570 KL=L.LT.2
5580 GR=L.GT.5
5590 FS=0.
5600 DO 233 I=1,N
5610 V=DT(I,1)
5620 C=(YM(I)+YL(I)+G*DY(I))*.5
5630 DT(I,1)=C
5640 TA=C
5650 IF(KL) GO TO 233
5660 DO 231 K=2,L
5670 B1=D(K)*V
5680 B=B1-C
5690 W=C-V
5700 U=V
5710 IF(DABS(B).LT.1E-9)GO TO 230
5720 B=W/B
5730 U=C*B
5740 C=B1*B
5750 230 V=DT(I,K)
5760 DT(I,K)=U
5770 231 TA=U+TA
5780 IF(.NOT.KONV)GO TO 232
5790 IF(DABS(Y(I)-TA).GT.S(I)*ETA)KONV=.F.
5800 232 IF (GR.OR.DABS(S(I)).LT.1E-9)GO TO 233
5810 FV=DABS(W)/S(I)
5820 IF(FS.LT.FV)FS=FV
5830 233 Y(I)=TA
5840 IF(DABS(FS).LT.1E-9) GO TO 250
5850 FA=FY
5860 K=L-1
5870 FY=(EP(K)/FS)**(1./FLOAT(L+K))
5880 IF(L.EQ.2) GO TO 240
5890 IF(FY.LT.0.7*FA)GO TO 250
5900 240 IF(FY.GT.0.7)GO TO 250
5910 H=H*FY
5920 JTI=JTI+1
5930 IF(JTI.GT.5)GO TO 30
5940 GO TO 10
```

```
5950 250 IF(KONV) GO TO 20
5960 D(3)=4.
5970 D(5)=1.6E01
5980 BO=.NOT.BO
5990 M=JR
6000 JR=JS
6010 260 JS=M+M
6020 H=H*.5
6030 GO TO 10
6040 20 X=XN
6050 H=H*FY
6060 RETURN
6070 30 H=0.
6080 DO 300 I=1,N
6090 300 Y(I)=YA(I)
6100 RETURN
6110 END
```

REFERENCES

Alexeev, I.I. and A.P. Kropotkin, Interaction of energetic particles with the neutral layer of the magnetospheric tail, Geomagn. Aeron. 10, 615-619, 1970.

Bulisch, R. and J. Stoer, Numerical treatment of ordinary differential equations by extrapolation methods, Numerische Mathematik 8, 1-13, 1966.

Cowley, S.W.H., The adiabatic flow model of a neutral sheet, Cosmic Elect., 2, 90-104, 1971.

Eastwood, J.W., Consistency of field and particle motion in the 'Speiser' model of the current sheet, Planet. Space Sci. 20, 1555-1568, 1972.

Eastwood, J.W., Some properties of the current sheet in the geomagnetic tail, Planet. Space Sci. 23, 1-14, 1975.

Gear, C.W., Numerical Initial Value Problems in Ordinary Differential Equation, Prentice Hall, 1971.

Hull, T.E., W.H. Enright, B.M. Fellen, and A.E. Sedgewick, Comparing numerical methods for ordinary differential equations, J. SIAM Numer. Anal., 9, 603-637, 1972.

Hull, I.E. and W.H. Enright, Test results on initial valve methods for non-stiff ordinary differential equations, J. SIAM Numer. Anal. 13, 944-961, 1976.

Kan, J.R., On the structure of the magnetotail current sheet, J. Geophys. Res. 78, 3773-3781, 1973.

Pudovkin, M.I. and N.A. Tsyganenko, Particle motions and currents in the neutral sheet of the magnetospheric tail, Planet. Space Sci. 21, 2027-2037, 1973.

Sonnerup, B.U.O., Adiabatic particle orbits in a magnetic null sheet, J. Geophys. Res. 76, 8211-8222, 1971.

Speiser, T.W., Particle trajectories in model current sheets - I. Analytical solutions, J. Geophys. Res. 70, 4219-4226, 1965.

Speiser, T.W., Particle trajectories in model current sheets - II. Applications to auroraes using geomagnetic tail model, J. Geophys. Res. 72, 3919-3932, 1967.

Speiser, T.W., Conductivity without collisions or noise, Planet. Space Sci. 18, 613-622, 1970.

Stern, D.P., and P. Palmadesso, Drift-free magnetic geometries in adiabatic motion, J. Geophys. Res. 80, 4244-4248, 1975.

Stern, D.P., Adiabatic particle motion in a nearly drift-free magnetic field: application to the geomagnatic tail, Goddard Space Flight Center Report X-602-77-89, 1977.

Stoer, J., Extrapolation methods for the solution of initial value problems and their practical realization, Lecture Notes in Mathematics, 362, Springer-Verlag, 1974.

Stormer, C. The Polar Aurorae, Oxford University Press, 1955.

Swift, D.W., The effect of the neutral sheet on magnetospheric plasma, J. Geophys. Res. 82, 1288-1292, 1977.

Toichi, T., Two-dimensional equilibrium solution of the plasma sheet and its application to the structure of the tail magnetosphere, Cosmic Electrodynamics 3, 81, 1972.